Integrated bio- and chemo-stratigraphy for Early Cretaceous strata offshore Gabon: Additional constraints on the timing of salt deposition and rifting of the South Atlantic

[1]James S. Eldrett, [2]Steven C. Bergman, [1]Christian Heine, [3]Paul Edwards, [3]Marcus Jakeman, [3]Nick Miles, [4]Bastian Hambach, [4,5]Steven, M. Bohaty, [4]Megan R. Wilding,

[1]Shell Global Solutions International B.V., Lange Kleiweg 40, 2288 GK Rijswijk, Netherlands

[2]SCB Geosciences, Vashon, Washington, USA

[3]PetroStrat Ltd., Tan-y-Graig, Parc Caer Seion, Conwy, LL32 8FA, UK

[4]School of Ocean and Earth Science, University of Southampton, National Oceanography Centre, Southampton SO14 3ZH, UK

[5]Institute of Earth Sciences, Heidelberg University, Im Neuenheimer Feld 234-236, 69120 Heidelberg, Germany

Keywords

Early Cretaceous, Gabon, Salt; Carbon isotope stratigraphy

Abstract

Early Cretaceous rift basins of the incipient South Atlantic have been the focus of intense hydrocarbon exploration and production activities and host some large oil accumulations in in sections predating an interval of major salt deposition, particularly in the central segment of the

South Atlantic. Understanding the timing (and associated uncertainties) of source rock and reservoir deposition and their relationship with rift evolution is critical for successful exploration. However, there are still many unresolved issues and data gaps regarding the precise age and duration of salt deposition. Better chronological constraints are particularly needed to the determine the timing of deposition of Pre-Salt reservoirs and the primary evaporites, as well as the secondary phase of halokinensis that resulted in variable reservoir sealing potential. To help address this gap, stable carbon isotope ($\delta^{13}C$) records from bulk organic matter and insoluble kerogen were generated for the Early Cretaceous salt and Pre-Salt intervals from two exploration wells offshore of Gabon. The bulk organic $\delta^{13}C$ stratigraphies for the two wells were then integrated with palynological and ostracod biostratigraphy and placed within a sequence stratigraphic and regional tectonic framework, providing new constraints on the timing of rift lake evolution and salt deposition. The good correlation between the offshore Gabon $\delta^{13}C$ record with other published sections calibrated to the current Geologic Time Scale as well as other regional sections from NE Brazil, supports the reliability of our new Gabon $\delta^{13}C$ record. Several $\delta^{13}C$ excursions are identified in the Pre-Salt sequence and are correlated with the Valanginian Weissert event and Early Aptian $\delta^{13}C$ event(s). Salt deposition on the Gabon margin is interpreted to have occurred during an interval straddling the Early-Late Aptian boundary (~118.4 to 116.8 Ma). These findings are comparable with other published estimates for salt deposition from northeast Brazil but differ from published estimates from the Campos-Santos basins; the latter are critically discussed. This study provides an important stratigraphic dataset for offshore Gabon and contributes to the ongoing debate regarding the timing of rifting and salt deposition in the Early Cretaceous of the South Atlantic passive margin system.

1. Introduction

The Early Cretaceous Epoch (Berriasian-Albian Stages; 143.1 Ma – 100.5 Ma; Gradstein *et al.* 2020) was a dynamic period in Earth history marked by globally evolving plate tectonic configurations associated with the final continental breakup of Gondwana, in particular rifting between South America and Africa and creation of the South Atlantic Ocean (Heine *et al.* 2013). The continental breakup of Gondwana involved complex mantle plume head-induced lithosphere interactions leading to fluctuating magmatic budgets including the emplacement and subsequent weathering of several Large Igneous Provinces (LIPs; Bodin *et al.* 2015; Johanson *et al.* 2018; Bergman *et al.* 2021). These mantle melting processes exerted first-order control on carbon outgassing from the deep Earth into the atmosphere, triggering responses in the biosphere and hydrosphere, and driving major perturbations in the surface carbon reservoir as expressed by global changes in climate and environmental conditions in both marine and continental realms (Hay, 2017; Brune *et al.* 2017; Lee *et al.* 2016; Black and Gibson, 2019; Mather and Schmidt, 2021). Although the Early Cretaceous was generally characterized by a greenhouse climate state with high atmospheric CO_2 concentrations (2-10 times present-day: Royer *et al.* 2010; Wang *et al.* 2014; Foster *et al.* 2017) and warm global temperatures (Huber *et al.* 2002, Mutterlose *et al.* 2010; Littler *et al.* 2011, Friedrich *et al.* 2012; O'Brien *et al.* 2017; Steinig *et al.* 2020; Scotese *et al.* 2021), it is clear that the warm, stable climate conditions were not maintained throughout the entire Early Cretaceous (see Bodin *et al.* 2015). Instead, the warm and equable Cretaceous greenhouse climate state was punctuated by periods of both (i) cooler conditions (Price *et al.* 2000; Kessels *et al.* 2006) with improved oxygenation of the water-column (Bralower *et al.* 1993) and even transient localized high latitude/altitude glaciations (Alley *et al.* 2019), and (ii) extreme warmth (Littler *et al.* 2011; O'Brien *et al.* 2017) with multiple phases of globally recognized dysoxic to anoxic conditions in the water column and deposition of marine organic-rich sediments, termed Oceanic Anoxic Events (OAE’s; Schlanger and Jenkyns, 1976; see review in Jenkyns, 2010).

One of the most significant of the Cretaceous OAE's occurred during the Early Aptian (OAE-1a; ~ 120 Ma) associated with magmatic degassing from the Greater Ontong-Java Plateau LIP (Percival *et al.* 2021) and marked by a rapid negative carbon isotope ($\delta^{13}C$) excursion followed by a long-lasting positive shift (Menegatti *et al.* 1998), as well as osmium isotope ($^{187}Os/^{188}Os$) anomalies supporting nearly a million year period of continual hydrothermal weathering of very large quantities of mafic and ultramafic rocks during a major phase of submarine LIP emplacement (Dickson *et al.* 2021). Additional OAE's are recorded in the Valanginian (Weissert event; Weissert *et al.* 1998, Gröcke *et al.* 2005) and Late Aptian – Early Albian (OAE-1b set), both expressed by $\delta^{13}C$ excursions and deposition of organic-rich sediments (Bralower *et al.* 1993). The record of these Early Cretaceous OAE's is mainly documented in marine paleo-shelf sequences around the globe where the sedimentary successions contain marine microfossils that have been robustly calibrated to the international Geologic Time Scale (GTS2020; Gradstein *et al.* 2020). Terrestrial records of Early Cretaceous OAE's are greatly under-represented compared to the marine records, which is partly a reflection of the challenges in dating of continental sequences that are often barren of age-diagnostic microfossils. However, improved stratigraphic techniques such as carbon isotope stratigraphy, geochronology and radiometric dating have enabled greater stratigraphic resolution and calibration of terrestrial records, including recently published records from the Arctic (Herrle *et al.* 2015, Vickers *et al.* 2016) and SE Asia (Zhang *et al.* 2016, 2021). In addition, the discovery of prolific oil reserves in the Lower Cretaceous continental sequences that underlie an interval of thick salt deposits (termed Pre-Salt) of the South Atlantic has led to a rapid increase in the number of exploratory wells with studies and publications documenting the response of the terrestrial ecosystem to these carbon cycle perturbations (i.e. Saller *et al.* 2016; Sabato Ceraldi and Green, 2017; Farias *et al.* 2019, Pietzsch *et al.* 2018, 2020; Tedeschi *et al.* 2017, 2019; Lúcio *et al.* 2020; Szatmari *et al.* 2021; Varejão *et al.* 2021). However, despite attention received in previous work, uncertainties in the age of sedimentary successions remain. In particular, the age of salt deposition is unresolved and potentially diachronous, with widely ranging estimates from the Early Aptian (~121 Ma) to Early Albian (100 Ma) when using absolute dates based on the GTS2020 (Gradstein *et al.* 2020). These age estimates are based on various techniques, such as (i) correlating continental microfossils (i.e., pollen and spores) to calibrated marine sections elsewhere (e.g. Doyle *et al.* 1977; 1982; Doyle, 1992; Grosdidier *et al.* 1996; Bate, 1999); (ii) occurrences of marine microfossils in supra-evaporite sedimentary sequences (Koutsoukos *et al.* 1993; Davison, 2007; Bengtson *et al.* 2007, 2018; Tedeschi *et al.* 2017; Lima *et al.* 2019; Campbell *et al.* 2019; Arai and Assine, 2020; Sanjinés et al. 2022); (iii) radiometric ages of volcanic rocks (Dias, 1994; Gomes *et al.* 2015; Szatmari and Milani, 2016; Szatmari *et al.* 2021); (iv) carbon isotope stratigraphy (Tedeschi *et al.* 2017, 2019; Pietzsch *et al.* 2020; Bastos *et al.* 2020; Varejão *et al.* 2021) and (v) rhenium-osmium (Re-Os) isotopic ages of black shales (Lúcio *et al.* 2020). The age of salt deposition is important as it marks the late rift phase transition from continental to marine deposition in the low latitude South Atlantic and provides the sealing potential where present to the Pre-Salt lacustrine reservoirs and source rocks. Better constraint on the age of salt deposition is also important as it ultimately governs the depositional window and potential accommodation space available for the deposition of the Pre-Salt hydrocarbon system, depending on the tectono-thermal age of underlying crust formation. In addition, more precise dating of these sequences not only allows better constraints on the timing and rates of extensional tectonism and thermal history (i.e., rift-drift transition, early margin hyperextension) and associated impact on hydrocarbon play elements but also provides a deeper understanding of the mechanisms and processes driving Early Cretaceous climate dynamics and the terrestrial ecosystem response (including the timing of evolution and migration of plant groups, notably angiosperms and gnetophytes).

To address some of these outstanding issues regarding Early Cretaceous basin development, depositional history, and rift evolution in the low-latitude South Atlantic, this study focuses on the stratigraphy of terrestrial fauna (ostracods) and flora (pollen/spores, freshwater algae and dinoflagellate cysts) of the Pre-Salt sequences of offshore Gabon (**Figure 1**) and provides detailed carbon isotope records for correlation and calibration to GTS2020 (Gradstein *et al.* 2020).

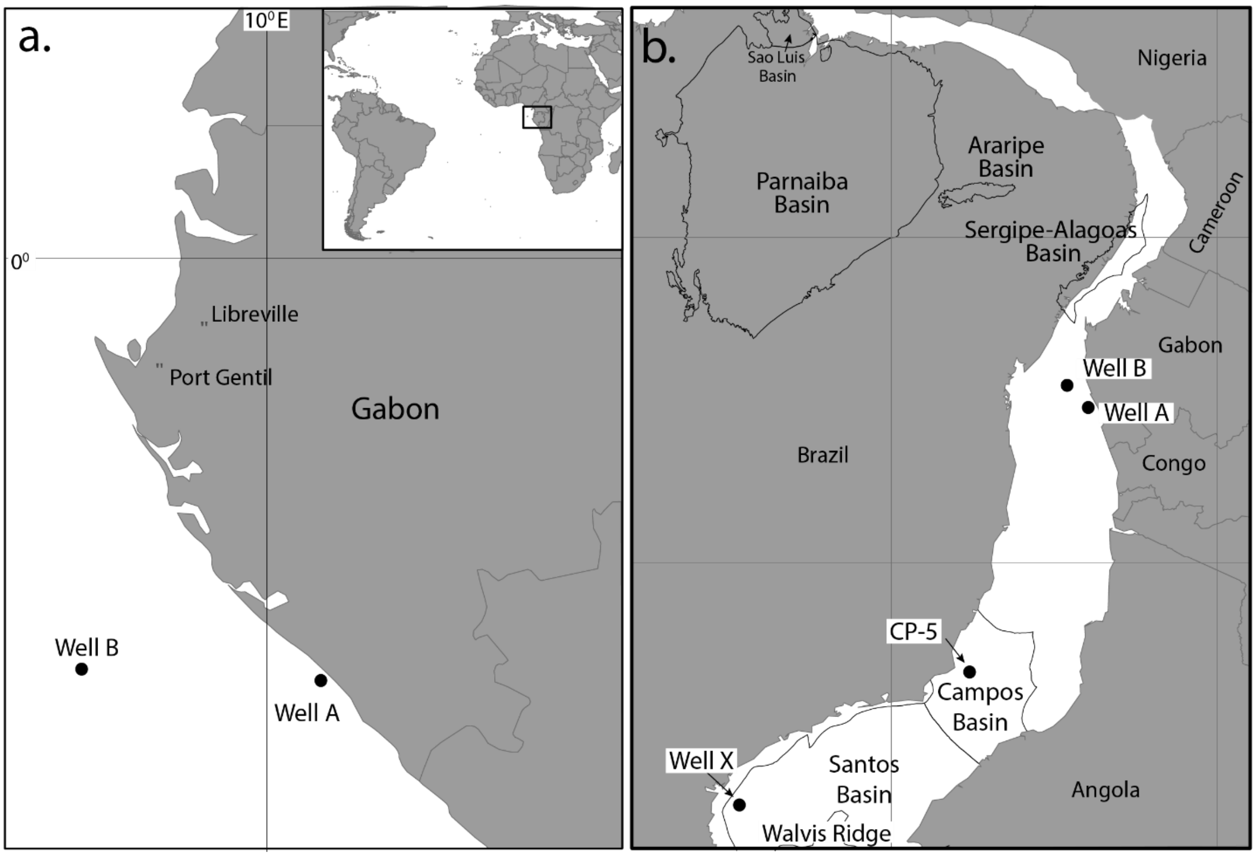

Figure 1. a. Location map showing the locations of wells A and B, offshore Gabon. **b.** Plate kinematic reconstruction (118 Ma) of the main basins and wells that are referred to in the text.

2. Geological Background

2.1. Stratigraphy of Gabon

Mesozoic rift basin formation in Gabon was linked by an extensive system of intra-continental rift basins to the global plate boundary network (Muller *et al.* 2019; Heine *et al.* 2013). Evidence from the South Atlantic, NE Brazilian, Central African and Equatorial African rift basins document an onset of continental extension in the Late Jurassic to earliest Cretaceous, which progressed to mature rifting and subsequent passive margin formation and continental breakup along the South and Equatorial Atlantic rifts, punctuated by mantle plume interaction in the Santos-Namibe Basin segment (Heine and Brune, 2014; Heine *et al.* 2013 and references therein). Breakup of the South Atlantic did not occur in a zipper-like fashion from South to North (as proposed by Rabinowitz and LaBrecque, 1979; Scotese *et al.* 1988; Fairhead, 1988, Torsvik *et al.* 2009; Moulin *et al.* 2010) but rather progressed from both ends. The western Benue (now overlain by the Niger delta) opened southwards and the southern South Atlantic opened northwards, with final breakup in the South Atlantic occurring in the Santos-Namibe segment in the Late Aptian (Heine *et al.* 2013; Neuharth *et al.* 2021). Together with the NE Brazilian Recôncavo Basin, the North Gabon Coastal Basin likely formed a continuous depocentre during the initial rift phase, before a change in rift kinematics in Barremian times led to the development of the Sergipe-Alagoas-Rio Muni rift branch, along which final breakup between Africa and South America occurred. During the rift phase, the North Gabon basin was filled by fluvial, deltaic, and lacustrine depositional systems and eventually capped by thick (<1-2 km) salt deposits prior to final breakup.

The Pre-Salt basin infill in the Gabon Basin encompasses the “Cocobeach series” and can be divided into four groups: i) Kango; ii) Remboué; iii) N'Toum and iv) N'Zeme Asso. These groups are illustrated in **Figure 2** and briefly described below:

i) The Kango Group represents the early infill of semi-isolated sub-basins within extensional fault-controlled grabens and half-grabens and is comprised of coarse-grained alluvial siliciclastic strata (the Basal Clastic / Vandji Formation [Fm.], c. 200-

500 m thick) overlain by mudstone-dominated deep-lacustrine facies (Kissenda Fm.; c. 1000-1500 m thick; Bate, 1999).

ii) The Remboué Group is marked at the base by Lucina lacustrine turbidite sandstones (Smith, 1994) and overlain by the lacustrine shales and sands of the Melania Fm (*ca*. 800 m thick). The Melania Fm. is subdivided into a lower Sandstone Member (Mb.) and an upper organic rich Shale Mb. (containing fewer interbedded thin sandstones).

iii) The N'Toum Group comprises Cardita Fm. mudstones characterized by lower organic matter contents. which are overlain by fluvial-deltaic sandstones-mudstones of the Dentale Fm., which together have been documented to be ~800-900 m thick. The Dentale Fm. is assigned to the Barremian Stage (Doyle, 1992; Bate, 1999).

iv) The N'Zeme Asso Series corresponds to the Coniquet and Gamba Fms. The Gamba Fm., with variable thicknesses (30-500 m), is a transgressive unit distributed throughout the Gabon and Congo Basins (Chela Fm.). The Gamba Fm. and the top of the Pre-Salt strata were originally assigned to the Early Aptian Stage (Doyle et al. 1977; Bate, 1999) although they were subsequently proposed to correspond to the Late Aptian by Poropat and Colin (2012). The Gamba Fm. disconformably lies on various lower units of the Cocobeach series except in a limited area in North Gabon, where the fluviatile sands and green clays of the Coniquet Fm. are apparently interbedded (Doyle *et al.* 1977). The Gamba Fm. can be divided into two members: a fluvial dominated sandstone interval (Gamba Sandstone Mb.) and a lagoonal mudstone interval (Vembo Shale Mb.) at its top interbedded with anhydrite and halite beds that mark the conformable transition to the overlying salt sequence of the Ezanga Fm. (JE personal observation).

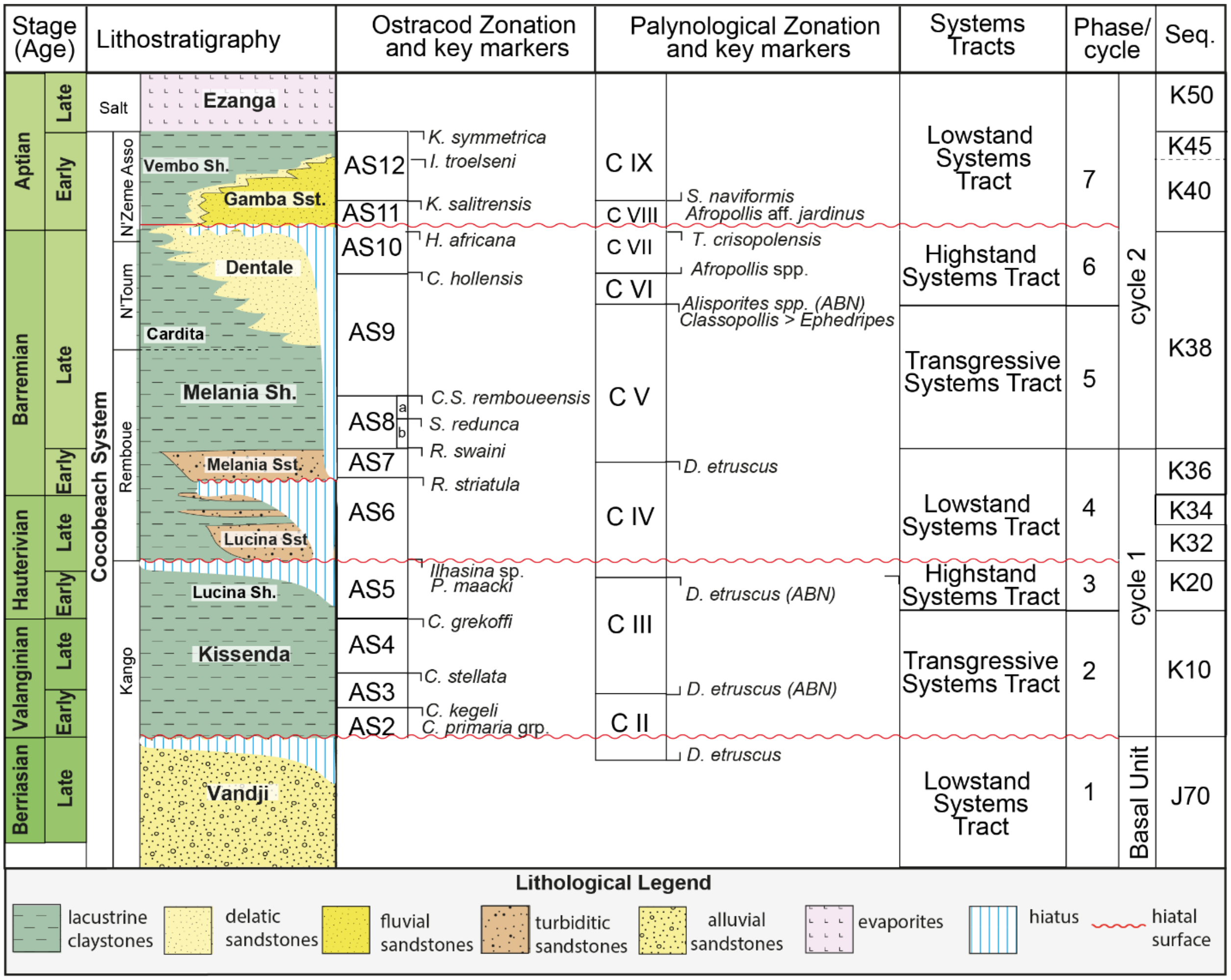

Figure 2. Stratigraphic scheme for Gabon Basin. Lithostratigraphy and ostracod zonation after Bate (1999); palynological zonation after Doyle *et al.* (1977) and Grosdidier *et al.* (1996); systems tracts, phase and cycle scheme after Bate (1999) and sequences (Seq.) applied following Copestake *et al.* (2003). Chronostratigraphic (Stage) calibration based on Bate (1999).

3. Material and Methods

One hundred and fifty-nine (159) ditch-cutting samples spanning the salt and Pre-Salt sequences in offshore Gabon were collected from wells A and B. Samples from Well A span the Kissenda Fm. to the Dentale Fm., overlain by a thin interval questionably assigned to the Gamba

Fm. Samples from Well B span the uppermost Dentale, Gamba and Ezanga Fms. All samples were washed and dried at wellsite and/or onshore at the Nederlandse Aardolie Maatschappij (NAM) core store in Assen, Netherlands to remove any drilling contamination by oil-based mud or hydrocarbons.

Biostratigraphic sample preparation and analyses were undertaken at Petrostrat Ltd, U.K. Samples for palynological analyses were subjected to the standard palynological preparation procedures, which involved removal of all mineral material by cold 30% hydrochloric acid followed by digestion in 60% hydrofluoric acid. The resulting residues were then concentrated by sieving through 10 µm and 20 µm nylon mesh screens. Aqueous strew mounts of each residue fraction were then air-dried on glass coverslips and mounted onto glass slides using Elvacite for each sample. Approximately 200 palynomorphs were counted with the rest of the slide scanned for rarer taxa.

Samples analyzed for ostracod assemblages were carefully disaggregated with limited physical processing to clean the samples and to limit damage to fragile ostracod tests (ostracod specimens are prone to mechanical damage caused by vigorous physical washing/sieving techniques). Where sample size allowed approximately 100 grams of material were soaked in water for approximately 48 hours. The residue from each sample was sieved into four fractions namely, >500 µm, <500 - 250 µm, <250 - 125 µm and <125 µm. The residue from each sieved fraction was spread on a picking tray and all microfossils were picked and deposited into a slide for analysis. All specimens picked were quantitatively logged. The unpicked residue was then scanned to check for the presence of any further marker species.

All ostracod and palynological species stratigraphic marker events are designated as last occurrence (range top, evolutionary extinction, or first downhole occurrence when drilling) and first occurrence (range base, evolutionary inception, or last downhole occurrence when drilling) datums.

Bulk organic stable carbon isotope ($\delta^{13}C$) and nitrogen isotope ($\delta^{15}N$) analyses were undertaken in the Stable Isotope Ratio Mass Spectrometry Lab at the University of Southampton, U.K. Selected mudstone chips from the samples were ground using an agate mortar and pestle, weighed and decarbonated with 10% hydrochloric acid, and then washed with deionized water until a solution pH of ~7 was achieved. The samples were then dried and re-weighed before isotopic analyses were performed on the acidified samples. In order to assess the influence of mixing of kerogen with more labile bulk organic matter in the Gabon Basin samples, $\delta^{13}C$ and $\delta^{15}N$ values were also determined for kerogen material that was isolated in representative samples from Well B. Kerogen was isolated in these representative samples through sequential dissolution in 60% hydrofluoric acid followed by 30% hydrochloric acid. The samples were then washed twice with deionized water to achieve a solution pH of 6-7 before being dried.

Bulk organic $\delta^{13}C$ and $\delta^{15}N$ values were determined using an Elementar vario Pyrocube elemental analyzer running in CNS mode and equipped with a TCD (thermal conductivity detector) coupled to an Isoprime VisION continuous flow isotope ratio mass spectrometer (IRMS). The samples were weighed out in clean tin capsules on a Sartorius ME5 micro balance and were then combusted at 1120°C with addition of pure oxygen. The resulting NOx and CO_2 gases were subsequently reduced to N_2 and CO_2 in the reduction column, which was held at 850°C. The elemental ratios were determined by the TCD and the isotope ratios by the IRMS analysis.

Acetanilide and sulfanilamide were used as an elementary standards for percentage (%) carbon and % nitrogen calibration. The stable isotope calibration and reporting methods follow the recommended best practices of Szpak *et al.* (2017) as follows. Carbon and nitrogen stable isotopic compositions were calibrated relative to the Vienna Pee Dee Belemnite (VPDB) and AIR scales using the international reference materials USGS40 and USGS41 (United States Geological Survey, Reston, VA, USA). Measurement uncertainty was monitored using suitable internal quality-control materials including the High Organic Sediment Standard OAS ($\delta^{13}C$

−26.67 ± 0.08‰, $\delta^{15}N$ +4.82 ± 0.17‰). Precision (u(Rw)) was determined to be ± 0.22‰ for $\delta^{13}C$ and ± 0.4‰ for $\delta^{15}N$ based on repeated measurements of calibration standards, check standards, and sample replicates. Accuracy or systematic error (u(bias)) was determined to be ± 0.09 for $\delta^{13}C$ and ± 0.2 for $\delta^{15}N$ based on the difference between the observed and known $\delta^{13}C$ and $\delta^{15}N$ values of the check standards and the long-term standard deviations of these check standards. The standard analytical uncertainty (Uc) was estimated to be ± 0.24‰ for $\delta^{13}C$ and ± 0.46 for $\delta^{15}N$. All calculations following the template of Szpak *et al.* (2017) and values are provided in the supplemental datafile. Carbon: nitrogen (C:N) ratios for the samples were calculated from the standard weight.

The newly generated bulk organic $\delta^{13}C$ values for the Gabon wells are compared to a composite Tethyan carbonate $\delta^{13}C$ reference curve (Herrle *et al.* 2004, 2015) and regionally available organic $\delta^{13}C$ curves (Ando *et al.* 2002; Herrle *et al.* 2015, Vickers *et al.* 2016). All of the $\delta^{13}C$ values were calibrated to GTS2020 (Gradstein *et al.* 2020). For the Aptian-Barremian interval this study applies the $\delta^{13}C$ zone/segment nomenclature (C1–C8) defined by Menegatti *et al.* (1998) and subsequent $\delta^{13}C$ zone/segments (C9 - C14) of Bralower *et al.* (1999).

4. Results

4.1. Palynological Results

The palynofloras from both Well A and Well B are dominated by terrestrially derived pollen and spores, specifically *Classopollis* gymnosperm pollen, associated with subordinate abundances of *Ephedripites* and *Araucariacites australis*. Fern spores such as *Deltoidospora* and *Cyathidites* are poorly represented. The Melania and Dentale Fms. contain relatively high abundances of algal cysts and the brackish/freshwater alga *Botryococcus braunii*, with influxes of freshwater dinoflagellate cysts (*Spicadinium* spp. and *Loboniella hirsuta*). Occasional marine dinoflagellate cysts (*Subtilisphaera* spp. and *Spiniferites ramosus*) are recorded from the mudstones of the Ezanga Fm. and are considered *in situ*. Key palynological marker species and events are identified, enabling the assignment to both wells of the West African palynological zonation (after Doyle *et al.* 1977; Grosdidier *et al.* 1996). These are illustrated in **Figures 3** and **4** and are as follows:

- Relatively low abundances of *Dicheiropollis etruscus* between 1200-1314.3 m in Well A (Kissenda Fm.) compared to the overlying strata are indicative of Palynological Zone C II.
- The high abundances of *Dicheiropollis etruscus* between 1103-1180 m in Well A (Kissenda Fm.) are indicative of Palynological Zone C III.
- The last occurrence of *Dicheiropollis etruscus* at 935 m in Well A (Melania Fm.) is the marker for the top of Palynological Zone C IV.
- Common abundances of the bisaccate pollen grains of the genus *Alisporites* with the first occurrence of *Stellatopollis hughesii* at 490 m define Palynological Zone C V in Well A (Melania Fm.).
- The first occurrence of *Tucanopollis crisopolensis* is identified within Palynological Zone C VI (Doyle *et al.* 1977); in Well A it occurs at 330 m within the Dentale Fm.
- The continued occurrence of *Tucanopollis crisopolensis* (Well A, 40m; Well B, 920 m) and a reduction in the abundance of *Alisporites* spp. (Well A, 130 m) and are used to recognize Palynological Zone C VII, corresponding to the Dentale Fm. In Well A, this interval also contains specimens attributed to *Afropollis aff. jardinus sensu* Doyle et al. (1982), which are interpreted as potentially caved downhole from younger strata above. However, if *in situ,* these occurrences would indicate an older range for *Afropollis* aff. *jardinus sensu* Doyle et al. (1982).

- Palynological Zone C VIII is based on the interval between the last occurrences of *T. crisopolensis* and *Alisporites* spp., and the first occurrence of *Sergipea naviformis*, with high abundances of *Classopollis* spp. and *Exesipollenites tumulus* (Well A, 40-0 m; Well B; 800-872 m).

- The occurrences of *Pennipollis peroreticulatus*, *Sergipea naviformis* and *Afropollis* aff. *jardinus sensu* Doyle et al. (1982) in the Gamba–Ezanga Fms. within Well B are used to identify this interval as Palynological Zone IX (773-60 m). Occurrences of other notable species include *Stellatopollis barghoornii* and *Sergipea variverrucata.*

4.2. Ostracod Results

The recovery of ostracod assemblages in Well A is variable. The basal section (Kissenda – Melania Fms.) contains low ostracod abundance, mostly comprising undifferentiated pyritized internal casts, whereas abundance is higher within the overlying Dentale Fm. Numerous marker species are identified in Well A, enabling the assignment of the West African *Ante Salifères* (AS) ostracod zonation (Grosdidier *et al.* 1996; Bate, 1999). These are presented in **Figure 3** and are as follows:

- At the base of Well A (Kissenda Fm.), the isolated occurrence of *Cypridea* aff. *primaria* at 1285 m is tentatively assigned to Ostracod Zone AS2 (according to Bate, 1999) or AS3 (according to Grosdidier *et al.* 1996) and marks the Berriasian Stage (Poropat and Colin, 2012)

- The isolated occurrence of *Theriosynoecum commune* at 1225 m (Kissenda Fm.) is tentatively assigned to Ostracod Zone AS4 and corresponds with the Valanginian Stage (Poropat and Colin, 2012)

- Isolated occurrences of *Cyprídea ventronodata* (1200 m) and *Ilhasina torosa* (1065 m) in the Lucina Fm. are tentatively assigned to Ostracod Zone AS5 and mark the Hauterivian Stage (after Poropat and Colin, 2012).

- The range tops of *Reconcavona swaini* (855 m) and *Salvadoriella redunca redunca* (895 m) in the Melania Fm. are used to recognize Ostracod Zone AS7 to Subzone AS8a (Barremian Stage).

- The range top of *Cypridea (Sebastianites) remboueensis* (450 m) is used to identify this interval as belonging to Ostracod Subzone AS8b (Melania Fm.). Secondary markers identified include: *Coriacina coriacea* (range between 700 m and 765 m) and *Petrobrasia marfinensis* (range between 530 m and 600 m).

- The occurrences of *Cypridea hollensis* (between 120-450 m), *Cypridea loango* (315-430 m) and the last occurrence of *Theriosynoecum postangularis* (430 m) in the Dentale Fm. are used to define Ostracod Zone AS9 (120-430 m) and are Late Barremian in age (Poropat and Colin, 2012).

- The occurrences of *Hourcqia africana africana* and *Damonella tinkoussouensis* at 100 m may be indicative of Ostracod Zone AS10. The last occurrence *H. africana africana* is at the top of Zone AS10 (*sensu* Grosdidier 1996, Bate 1999), and as shallower depths were not analyzed in this study, the occurrences of *H. africana africana* in Well A are likely not to reflect the true last occurrence.

4.3. Stable Isotope Results

The $\delta^{13}C$ values range in Well A between -28 and -20‰, with numerous positive and negative $\delta^{13}C$ excursions recorded over short intervals throughout the section (**Figure 3**). Mean $\delta^{13}C$ values of ~-26‰ are recorded in the Kissenda Fm. (1190-1300 m), with a ~3‰ increase in the lowermost part of the section reaching peak values of ~-23‰ at 1235 m, before returning to background levels (~-26‰) in the Lucina Fm (1180-1030 m). The overlying Melania Fm. is marked by a sharp increase in $\delta^{13}C$ values (~1015 m) that remain high (mean -24‰) with several peaks near -20‰ (~640 m; ~555 m). The upper part of the Melania Fm., which is characterized by lower $\delta^{13}C$ values (-26 to -27‰; between 545-390 m), that increase in the basal Dentale Fm. reaching a maximum of -20‰ (350 m), before declining and stabilizing to around -25‰ in the upper Dentale Fm. (275-0 m). In Well A, $\delta^{15}N$ values range between 2 and 9‰, with slightly higher $\delta^{15}N$ values in the Kissenda-Lucina Fms. (mean = 7‰; 1300 - 970 m) compared to the Melania Fm. (mean 5.6 ‰; 1015-425 m) and Dentale Fm. (mean 4.7 ‰; 420-0 m).

In Well B, the Gamba Fm. is characterized by high $\delta^{13}C$ values in both bulk organic matter and kerogen material (-22 to -23‰; 886-420 m) that decrease in the Ezanga Fm., with mean $\delta^{13}C$ values of -27‰ (400-90 m; **Figure 4**). The $\delta^{13}C$ values from the Vembo Shale Mb. (Gamba Fm., ~580-~420 m) are consistent between bulk organic matter (ave. -22.7‰; σ = 0.6‰) and kerogen material (ave. -23.1‰; σ = 0.6‰). Several samples that were analyzed from Well B contained low nitrogen concentrations, preventing measurement of $\delta^{15}N$ values. However, for those sample that were possible to analyze in the Gamba Fm., $\delta^{15}N$ values are between 1 and 2‰. The overlying Ezanga Fm. exhibited slightly higher $\delta^{15}N$ values ranging from 5 to 7‰.

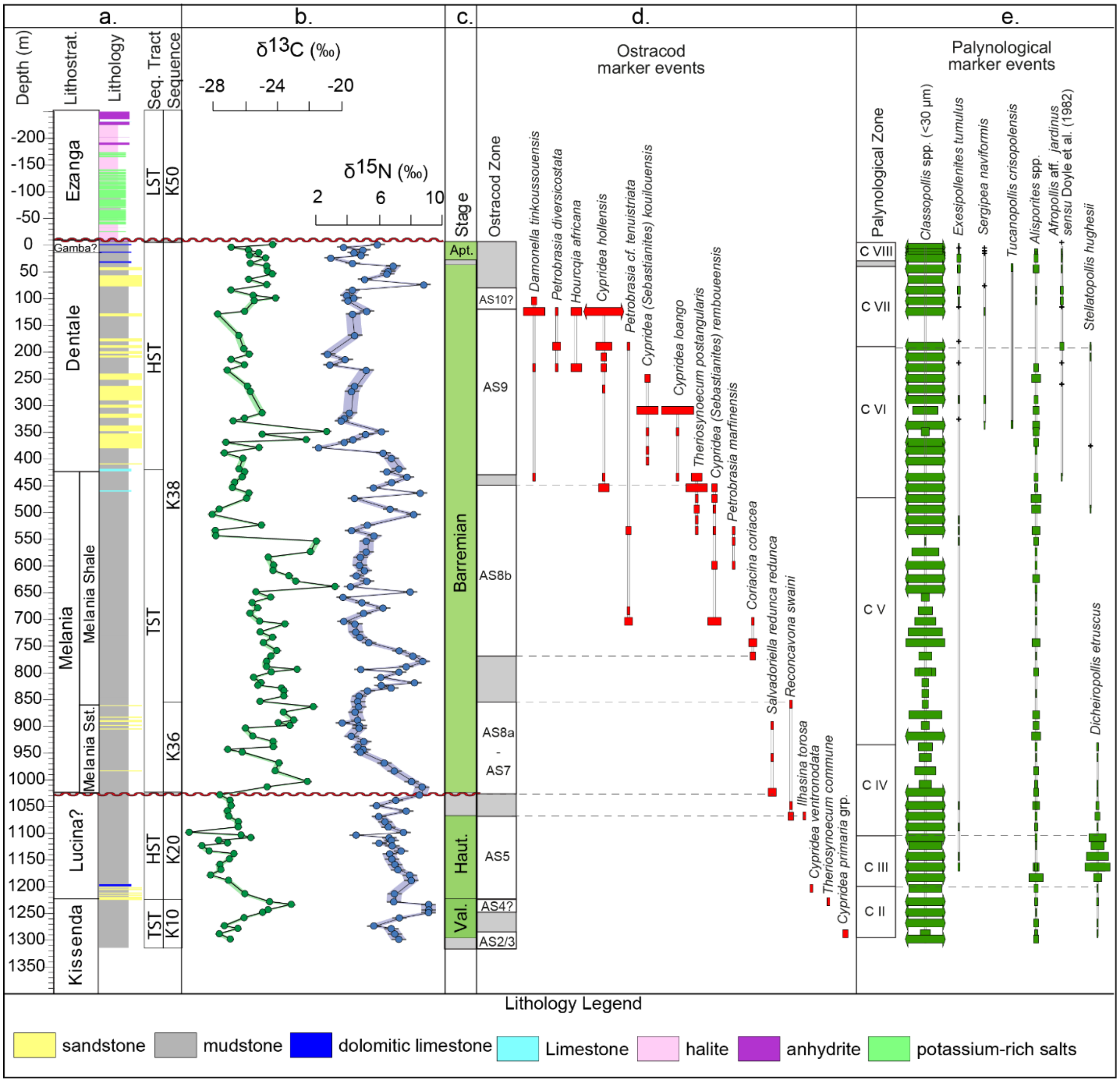

Figure 3. Summary of results for Well A. **a.** Lithostratigraphy, lithology (for key see legend panel) and sequence stratigraphic interpretation. **b.** Stable $\delta^{13}C$ and $\delta^{15}N$ values of bulk organic matter; standard uncertainty (U_c) represented by green and blue shading respectively. **c.** Interpreted chronostratigraphic stages based on the biostratigraphic data; **d.** Ostracod zonation after Bate (1999); Grosdidier *et al.* (1996) and Poropat and Colin (2012) with identified marker events and semi-quantitative ranges; **e.** Palynological zonation after Doyle *et al.* (1977); with

identified marker events and semi-quantitative ranges. Horizontal dashed lines represent zonal marker events; horizontal wavy red line represents hiatus.

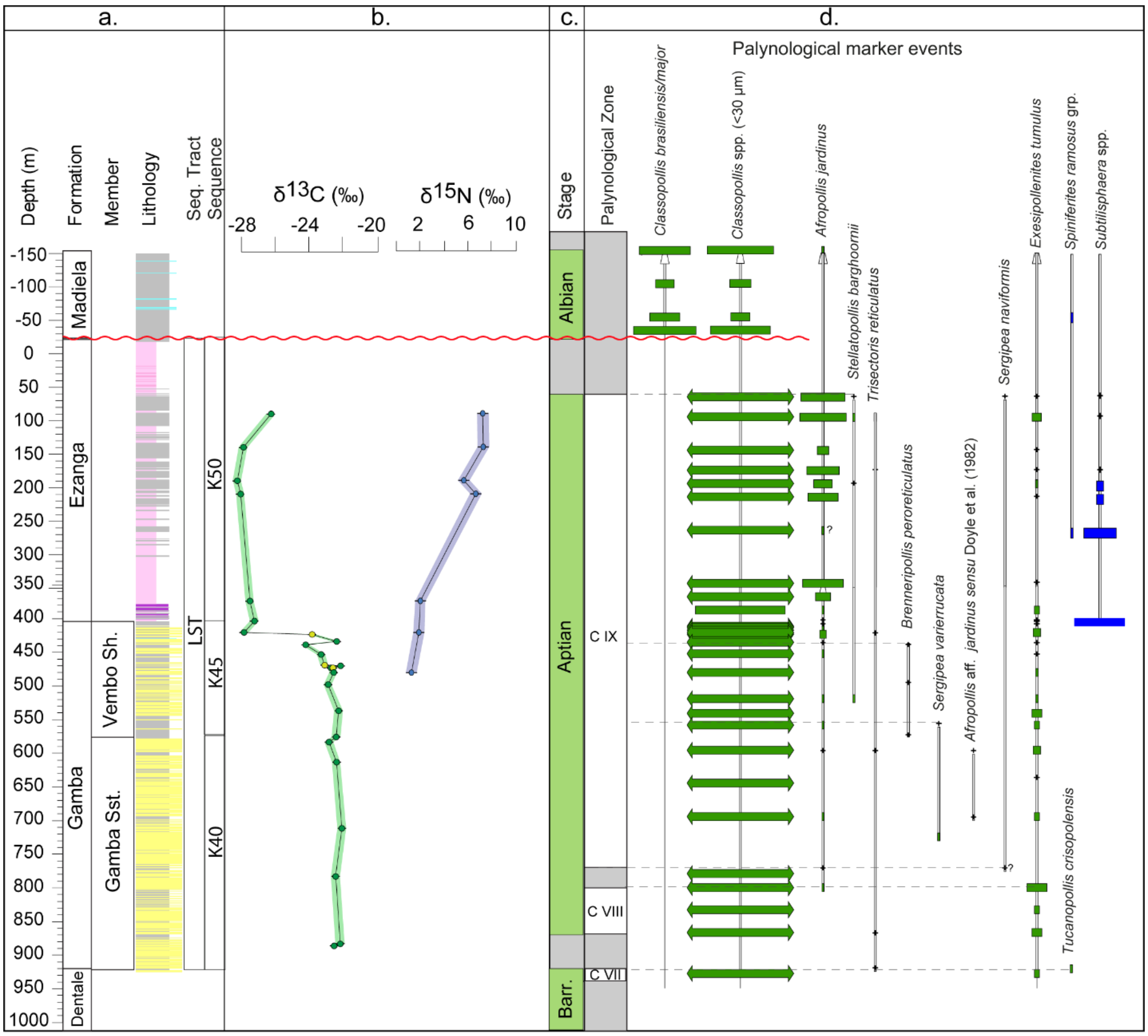

Figure 4. Summary of results for Well B. **a.** Lithostratigraphy, lithology (legend on Fig. 3) and sequence stratigraphic interpretation; **b.** Stable $\delta^{13}C$ values of bulk organic matter (dark green circles) and kerogen material (light green circles); $\delta^{15}N$ values (blue circles). Standard uncertainty (U_c) represented by green and blue shading respectively. **c.** Interpreted chronostratigraphic

stages based on the biostratigraphic data; **d.** Palynological zonation after Doyle *et al.* (1977); with identified marker events and semi-quantitative ranges. Horizontal dashed lines represent zonal marker events; horizontal wavy red line represents hiatus.

5. Discussion

5.1. Evaluation of carbon isotope values

Our study provides detailed stratigraphic data for the Early Cretaceous South Atlantic rift sequences from offshore Gabon. However, before ascertaining the possible global significance of the observed changes in the $\delta^{13}C$ values, potential diagenetic or local influences on the record must first be evaluated. Additionally, when measuring and analyzing $\delta^{13}C$ from hydrocarbon exploration or production wells it is critical that the samples represent borehole sediment material and do not record $\delta^{13}C$ variations resulting from either oil-based drilling mud or discovered hydrocarbon contamination. To address this point, the samples were thoroughly washed and cleaned at wellsite and/or at the NAM onshore core laboratory, which combined with the preparation process for EA-IRMS analysis (grinding, acidification, and rinsing) would remove or significantly reduce the potential impact of contamination. In addition, the comparison between bulk organic $\delta^{13}C$ and the kerogen $\delta^{13}C$ show similar values indicating that the bulk organic $\delta^{13}C$ is representative of the maceral component and not influenced by any excess carbon due to hydrocarbon additions (oil-based mud or produced).

The organic $\delta^{13}C$ values may also be affected by post-depositional influences such as recorded during post-depositional oxidation of organic matter during subaerial exposure (Oehlert and Swart, 2014), or during thermal alteration with burial (Tyson, 1995). In both cases, total organic matter content is reduced and the associated $\delta^{13}C$ values become more negative as labile organic matter is preferentially oxidized or thermally converted (Tyson, 1995; Oehlert and Swart, 2014).

This relationship should be reflected by a strong covariance between $\delta^{13}C$ and total organic carbon (Oehlert and Swart, 2014). For the studied wells, the comparison between $\delta^{13}C$ and total organic carbon fraction shows weak and insignificant covariation (r^2=0.002; p-value =0.58; **Figure 5a**) suggesting that the $\delta^{13}C$ values likely reflect conditions at deposition. This is supported by visual inspection of the kerogen, which shows good preservation of macerals, thus indicating limited post-depositional oxidation or thermal alteration. Furthermore, the macerals exhibit a light colouration, which combined with previously analyzed bulk rock pyrolysis data that record Tmax values consistently around ~434° for all samples (see Supplemental data) indicates relatively low thermal maturity of the organic matter (immature to earliest oil window). It is possible that some more labile organic matter may have been converted to hydrocarbons; however, as Tmax. values are consistent for all samples the effect of thermal maturity on the $\delta^{13}C$ values is assumed to be uniform and not be responsible for depth-specific shifts in the $\delta^{13}C$ records (artefactual $\delta^{13}C$ excursions).

The bulk organic $\delta^{13}C$ values may also be influenced by changes in organic matter source, which can be evaluated by the carbon: nitrogen (C:N) ratio of the organic matter (see review in Tyson, 1995). Generally, a covariance between $\delta^{13}C$ and C:N ratio reflects the mixture of aquatic ($\delta^{13}C$ ~-20‰; C:N = <20) and terrestrial ($\delta^{13}C$ ~-26‰; C:N = >30) organic matter (Tyson, 1995). In the studied wells, the measured $\delta^{13}C$ and C:N values range between -20‰ to -29‰, and 8-50, respectively, indicating a mixture of both terrestrial and aquatic organic matter. This is also confirmed by the palynological analyses, which indicate the organic matter is an admixture of continentally derived material comprising both terrestrially derived material (pollen, spores, phytoclasts) and aquatic matter (i.e., freshwater algae) with no evidence for marine macerals in the Pre-Salt sequences. The palynological assemblages from the intra-salt mudstones of the Ezanga Fm. have similar composition to the Pre-Salt sequences, being dominated by terrestrial palynomorphs with subordinate aquatic freshwater components; however, the occurrence of the dinoflagellate cysts *Subtilisphaera* spp. and *Spiniferites ramosus* is interpreted as being *in situ* and records the incursion of marine waters within the Ezanga Fm. Irrespectively, there remains a weak and insignificant covariance between $\delta^{13}C$ and the C:N ratio (r^2=0.001; p-value = 0.62; **Figure 5b**) indicating limited influence of organic matter source on the $\delta^{13}C$ values. Although the Early Cretaceous was prior to the evolution of C4 land plants (which are responsible for large variations in $\delta^{13}C$ and C:N values in the Neogene), the lack of $\delta^{13}C$ and C:N covariation indicate that shifts in hinterland vegetation, local aquatic floral composition (i.e. freshwater algal blooms) or marine organisms (dinoflagellate cysts) had limited impact of the bulk organic $\delta^{13}C$ record.

The relationship between $\delta^{13}C$ and $\delta^{15}N$ values can also provide insight into water column conditions, organic matter source and potential floral assemblage shifts between terrestrial and aquatic sources (see Robinson *et al.* 2012; Quan and Adeboye, 2021 and references therein). Based on the relatively low thermal maturity of the organic matter (as discussed above) and good organic matter/kerogen preservation state we assume that the measured $\delta^{15}N$ values also reflect primary organic values and are not significantly affected by post-depositional diagenesis (i.e., catagenesis and fluid migration), although isotopic alteration may have occurred at the sediment-water interface during early burial of sedimentary organic matter (Robinson *et al.* 2012).

There is also a weak and insignificant covariation between $\delta^{13}C$ and $\delta^{15}N$ values (**Figure 5c**), indicating that the $\delta^{13}C$ record was not linked to the nitrogen cycle through localized nutrient and biological activity (either aquatic in origin or through terrestrial additions) within the rift lacustrine system. The high variability in $\delta^{15}N$ values (**Figures 5c & 5d**) may reflect the various contributions and admixture of terrestrial and aquatic organic matter to the bulk $\delta^{15}N$ record. Specific contribution from terrestrial and aquatic organic matter to both $\delta^{15}N$ and $\delta^{13}C$ values could be further assessed by isolating and measuring the isotopic composition of individual macerals (i.e., van Roij *et al.* 2017) or compound-specific organic fractions of organic matter (Wang *et al.* 2015), which, although beyond the scope of this contribution, could form the basis for future studies.

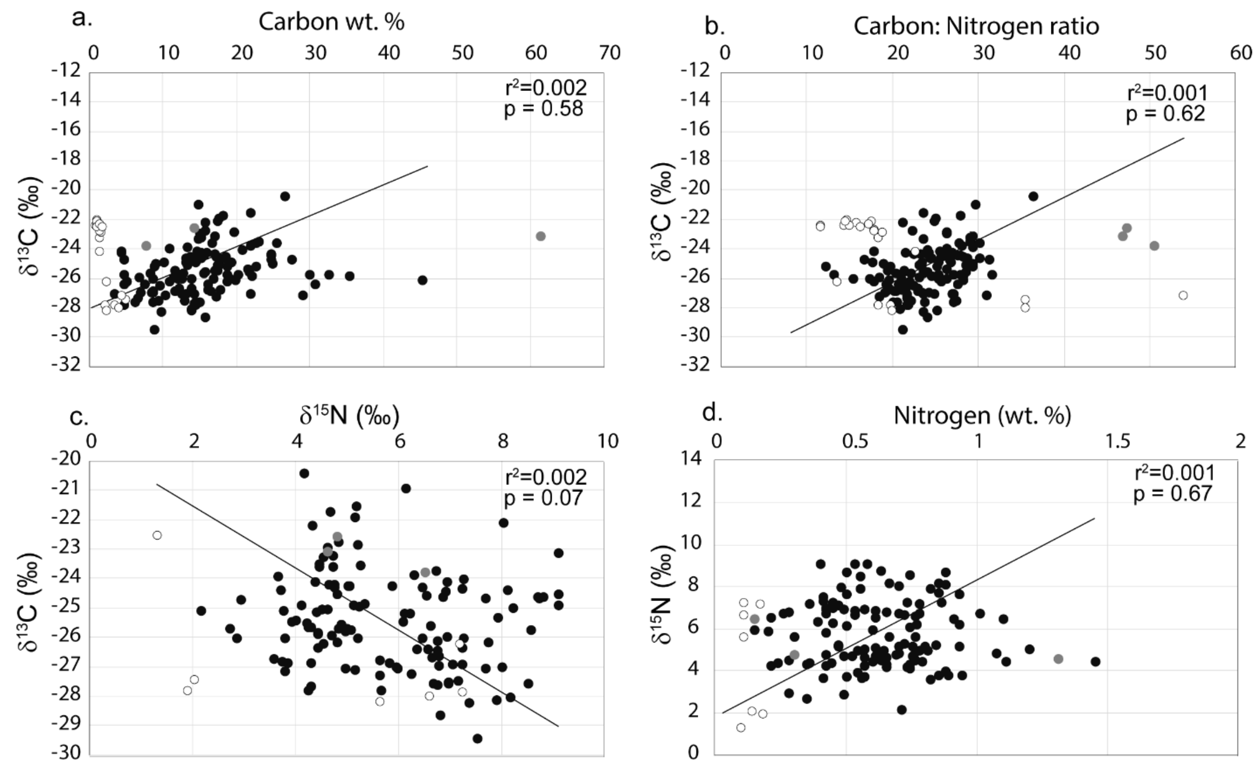

Figure 5. Stable isotope-geochemical cross plots showing **a.** relationship between $\delta^{13}C$ and total organic carbon (wt. %); **b.** $\delta^{13}C$ and carbon: nitrogen ratio**; c.** $\delta^{13}C$ and $\delta^{15}N$**; d.** $\delta^{15}N$ and total organic nitrogen (wt. %). Solid fill circles = bulk organic matter, Well A; Open circles = bulk organic matter, Well B; Grey filled circles = kerogen samples from Well B. Regression lines illustrated (solid black lines) after Reduced Major Axis Regression (RMA) with r^2 and p-value significance plotted with significance levels <0.05.

In addition to the above assessments on the potential controls on sedimentary $\delta^{13}C$ values, it should be noted that there is a close similarity between the trends in the offshore Gabon bulk organic $\delta^{13}C$ record and other $\delta^{13}C$ records from different basins and paleoenvironments, measured on both bulk and terrestrial organic matter (Ando *et al.* 2002; Herrle *et al.* 2015; Vickers *et al.* 2016; Tedeschi *et al.* 2019; Bastos *et al.* 2020). This similarity in $\delta^{13}C$ records further supports the proposition that localized organic matter source, contamination or post-depositional diagenesis did not significantly alter the carbon isotope record of the salt and Pre-Salt sequences, confirming the potential for their use in regional and global correlation and calibration.

5.2. Carbon Isotope Stratigraphy

To determine the regional and/or global significance of the $\delta^{13}C$ record generated for the salt and Pre-Salt sequences in offshore Gabon, the composite $\delta^{13}C$ profile from the two wells was compared with other Early Cretaceous sections that have detailed organic $\delta^{13}C$ records and are also constrained by either ammonite and/or marine microfossil biostratigraphy and/or radiometric ages (i.e., Gröcke *et al.* 2005; Herrle *et al.* 2015; Vickers *et al.* 2016; Tedeschi *et al.* 2019; Bastos *et al.* 2020). All the sections are also compared with the calibrated Tethyan composite $\delta^{13}C$ carbonate record (Herrle *et al.* 2015) and calibrated to GTS2020 (Gradstein *et al.* 2020; **Figure 6**).

The lowermost interval of the Gabon wells in the Kissenda Fm. is assigned to the Late Valanginian based on the occurrence of Ostracod Zone AS4 (Bate, 1999; Poropat and Colin, 2012). This interval also records a +3 ‰ positive $\delta^{13}C$ shift that is comparable to other terrestrial $\delta^{13}C$ records (Gröcke *et al.* 2005) and Tethyan carbonate $\delta^{13}C$ record (Herrle *et al.* 2015); we therefore attribute this excursion to the Late Valanginian Weissert $\delta^{13}C$ event. The overlying Lucina Fm. records a decrease in $\delta^{13}C$ values of similar magnitude to that recorded by Gröcke *et al.* (2005) in the Hauterivian of Crimea, Ukraine. This age assignment supported by the occurrence of Ostracod Zone AS5 (Poropat and Colin, 2012). The $\delta^{13}C$ profile from offshore Gabon provides an additional data point for the Valanginian-Hauterivian, a time interval with relatively scarce $\delta^{13}C$ records on organic matter, particularly in the low latitudes.

The shift in $\delta^{13}C$ values at the boundary between the Lucina Fm and Melania Fm, combined with the absence of Ostracod Zone AS6, is interpreted as reflecting a hiatal surface. This corresponds with a regional sequence boundary that elsewhere bounds the base of other lowstand lacustrine turbidites such as the Lucina Fm (Smith, 1994). The overlying Melania Fm. comprises a sandy lower interval (Melania Sandstone Mb.) and an upper organic-rich interval (Melania Shale Mb.) and is assigned to the Barremian based on the occurrence of Ostracod Zones AS7 – AS8 (see **Figure 3**). The $\delta^{13}C$ values of the Melania Fm. are relatively high (~-24‰) compared to the Lucina Fm., and similar to the Barremian $\delta^{13}C$ record from the northern high latitudes (Herrle *et al.* 2015; Vickers *et al.* 2016; **Figure 6**). The peak in $\delta^{13}C$ values (~-20‰; 555 – 640m) may correspond with the Mid Barremian Event identified in the Tethyan Realm (Coccioni *et al.* 2003), although this assignment is uncertain.

The bulk organic $\delta^{13}C$ record of the Dentale Fm. is more variable, with relatively low values at the base (~27‰) that increase -20‰ before stabilizing at around -25‰ at the top of the Dentale Fm. This interval is assigned to the Late Barremian to Early Aptian based on Ostracod Zones AS9 – AS10 and Palynological Zones C VI – C VIII (**Figure 3**). The stable $\delta^{13}C$ interval at the top of the Dentale Fm. is correlated to $\delta^{13}C$ Segment C2 (after Menegatti *et al.* 1998) and occurs within the Early Aptian. The Aptian-Barremian boundary is tentatively correlated to ~130m in Well A, based on comparison between the wellbore $\delta^{13}C$ stratigraphy and the Tethyan composite $\delta^{13}C$ carbonate record (Herrle *et al.* 2015) calibrated to GTS2020 (Gradstein *et al.* 2020). The Aptian-Barremian boundary would therefore correspond to an interval within Palynological Zone C VII, supporting both the original Aptian age assignment by Doyle *et al.* (1977; 1982) and the subsequent revision to the Late Barremian (Doyle *et al*. 1992). The $\delta^{13}C$ segments C3–C6 (corresponding with OAE-1a) are not recorded in the studied wells and are likely missing in a hiatal interval corresponding with the regional base Gamba unconformity (see Bate, 1999).

The Gamba Fm. in Well B is characterized by elevated $\delta^{13}C$ values (-22‰ to -23‰) that reach a plateau and are assigned to $\delta^{13}C$ Segment C7 (Menegatti *et al.* 1998), which is comparable to other global records (i.e., Ando *et al.* 2002; Herrle *et al.* 2015, Vickers *et al.* 2016; **Figure 6**). This interval corresponds with Palynological Zone C VIII to C IX; the latter includes the occurrence of *Sergipea variverrucata*, a marker that has been used to define the *Sergipea variverrucata* palynological zone (Regali *et al.* 1974) in NE Brazilian Basins and has recently also been calibrated to the $\delta^{13}C$ Segment C7 in the Sergipe-Alagoas Basin (Ibura Mb; Tedeschi *et al.* 2019) and Parnaiba Basin (Codo Fm; Bastos *et al.* 2020).

The lithological transition from the lagoonal shales of the Vembo Shale Mb. (Gamba Fm.) to the marine evaporites of the Ezanga Fm. is gradual and conformable. The $\delta^{13}C$ values decline across this interval and remain low (~-27‰) in the Ezanga Fm., which is correlated with the $\delta^{13}C$ Segment C8. This correlation would suggest that in the studied wells offshore Gabon, salt deposition initiated ~118.4 Ma (GTS2020; Gradstein *et al.* 2020; **Figure 6**). The shift to lower $\delta^{13}C$ values in the Ezanga Fm. may be influenced by a change in organic matter source, with the first occurrence of marine dinoflagellate cysts. However as discussed above, the overall organic matter type and palynological assemblages are similar to those in the underlying Pre-Salt sequences, which are both characterized by mixed continental sources (terrestrial and aquatic) and exhibit poor covariance between $\delta^{13}C$ and C:N values, suggesting that a marine incursion and any associated changes in local organic matter source did not significantly influence the $\delta^{13}C$ values.

It is possible that the regional-global carbon cycle and associated $\delta^{13}C$ values were impacted by the widespread deposition of evaporites in the South Atlantic. Initial geochemical models postulate that the widespread removal of seawater sulphate due to evaporite deposition in the South Atlantic would have reduced global concentration of sulfate, limiting the ability of sulphatereducing bacteria to demineralize organic matter and result in decreased pyrite burial and enhanced organic-matter preservation (Wortmann and Chernyavsky, 2007; Wortmann and Paytan, 2012). This relationship was used to explain both the initial negative sulphur isotope ($\delta^{34}S_{sulfate}$) and positive $\delta^{13}C$ shifts recorded during and immediately after OAE-1a ($\delta^{13}C$ Segment C7; Wortmann and Chernyavsky, 2007; Tedeschi *et al.* 2017). However, more recently Mills *et al.* (2017) applied a linked sulfur-strontium isotope mass-balance model that demonstrated marine sulfate concentrations increased significantly (rather than decreased as proposed by Wortmann and Chernyavsky, 2007) during the initial negative $\delta^{34}S_{sulfate}$ shift recorded during and immediately after OAE-1a. This model only reproduces the coupled negative sulfur and strontium isotope shifts when both hydrothermal and weathering fluxes increase during OAE-1a (linked with Greater Ontong-Java Plateau LIP; Percival *et al.* 2021), with evaporite deposition and reduced marine sulfate concentrations occurring later in the Aptian, corresponding with the long-term minima in $\delta^{34}S_{sulfate}$ and $\delta^{13}C$ values ($\delta^{13}C$ Segment C8; ~117 Ma; Mills *et al.* 2017). However, a discrepancy exists in that $\delta^{13}C$ Segment C8 is characterized by low $\delta^{13}C$ values, when the geochemical models suggest that reduced marine sulfate concentrations due to evaporite deposition would result in a positive $\delta^{13}C$ excursion due to decreased pyrite burial and enhanced organic-matter preservation (Wortmann and Chernyavsky, 2007; Wortmann and Paytan, 2012). Additional processes should be considered to explain how widespread evaporite deposition and reduced marine sulfate concentrations could potentially be responsible for the low $\delta^{13}C$ values recorded in the Ezanga Fm. and possibly the $\delta^{13}C$ Segment C8 globally. In the modern Ocean, anaerobic oxidation by sulfate is a major sink for methane (CH_4; D'Hondt *et al.* 2002; Valentine, 2002). As such, the reduction in seawater sulfate concentrations due to evaporite deposition would tend to promote methanogenesis in sulfate-depleted marine pore waters, eliminating anaerobic CH_4 oxidation as a major methane sink, and allow for the accumulation of ^{12}C-enriched CH_4 in the ocean and release to the atmosphere (Luo et al. 2010). The addition of ^{12}C-enriched CH_4 could potentially produce the lower $\delta^{13}C$ values that characterize both the Ezanga Fm. and $\delta^{13}C$ Segment C8.

The boundary between the upper Ezanga Fm. and the overlying marine carbonates of the Madiela Fm. is unconformable based upon biostratigraphic and seismic evidence from the Leopard prospect, offshore Gabon (Campbell *et al.* 2019). The occurrence of the planktonic foraminifera species *Microhedbergella rischi* and *M. renilaevis* in the basal Madiela Fm. overlying the Ezanga salt allows assignment of the corresponding $\delta^{13}C$ record to the latest Aptian to Early Albian OAE-1b $\delta^{13}C$ set (Campbell *et al.* 2019). The post-salt sequence generally compares with the Early to Middle Albian $\delta^{13}C$ record from the Tethys and Arctic (Herrle *et al.* 2015). For consistency with the C-segment nomenclature (after Bralower *et al.* 1999), the higher $\delta^{13}C$ values directly above the salt from the Leopard prospect (which were assigned to the OAE-1b $\delta^{13}C$ set by Campbell *et al.* 2019) would therefore potentially correspond to $\delta^{13}C$ Segment C11, with the subsequent up-section decrease corresponding with $\delta^{13}C$ Segments C13 – C14 (**Figure 6**). The assignment of the basal Madiela Fm. to the latest Aptian to Early Albian OAE-1b $\delta^{13}C$ segment C11 (Campbell *et al.* 2019) based on the biostratigraphic constraints precludes the possibility that the elevated $\delta^{13}C$ values currently assigned to the $\delta^{13}C$ Segment C7 (after Menegatti *et al.* 1998) from the deeper Gamba Fm. are from a younger $\delta^{13}C$ event.

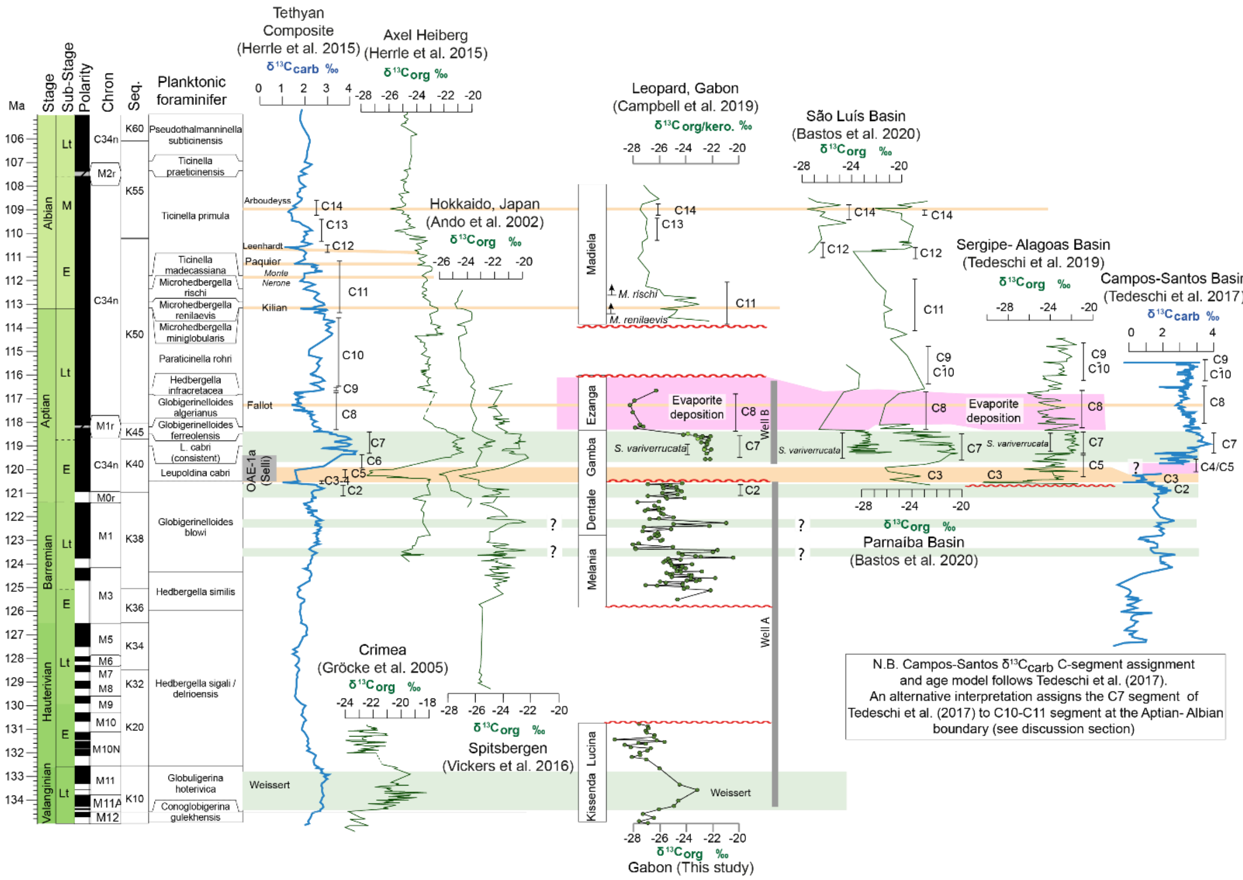

Figure 6. Comparison between δ^{13}C record from offshore Gabon (this study; Campbell *et al.* 2019) with the Tethyan composite carbonate δ^{13}C (Herrle *et al.* 2015) and organic δ^{13}C records (Ando *et al.* 2002; Herrle *et al.* 2015; Vickers *et al.* 2016) that are calibrated with the current international Geologic Time Scale (GTS2020; Gradstein *et al.* 2020). Relevant regional South Atlantic δ^{13}C records are also plotted for comparison (age models and δ^{13}C segment interpretations after Tedeschi *et al.* 2017, 2019; Bastos *et al.* 2020). The quality of the age model and Campos-Santos δ^{13}C composite profile after Tedeschi *et al.* (2017) is questioned here and should be treated with caution (see section 5.4). Green horizontal fill represents recognized positive carbon isotope excursions; tan horizontal fill represents recognized negative carbon isotope excursions; uncertain correlations are indicated with a question mark. Major OAE's are labelled alongside the Tethyan composite carbonate δ^{13}C profile. The main δ^{13}C segments after Menegatti *et al.* (1998) and Bralower *et al.* (1999) are also labelled (C2 to C14).

5.3. Sequence Stratigraphy

Early Cretaceous rift strata across the entire South Atlantic are subdivided into several mega-sequences/cycles by numerous authors. This paper does not intend to review all these contributions and will present only the key schemes that are relevant to this study (**Figure 2**). One of the first sequence stratigraphic schemes for the rift sequences of the South Atlantic was published by Bate (1999), who defined three mega-cycles for the West African margin. These are as follows:

(i) A Basal Unit comprising lowstand fluvial-alluvial deposits within shallow fresh-water lakes forming in the initial rift during the onset of continental stretching.

(ii) A first cycle reflecting the initial deepening of lakes due to increased lithosphere extension and accommodation space (transgressive phase; Kissenda Fm.), reaching a highstand phase; with the end of the cycle representing the lowstand deposits as either lakes infilled or lake-level dropped resulting in turbidite deposition (Melania and Lucina sandstone Mbs; see Smith, 1994)

(iii) A second cycle reflecting a further period of lake expansion (Melania Fm.) and subsequent infill (Dentale Fm.) as part of the transgressive to highstand sequence; ultimately followed by a lowstand system tract (LST). The LST is dominated by fluvial sediment infill (Gamba Fm.) culminating in evaporite deposition (Ezanga Fm/ Loeme Salt Fm.).

On the Brazilian margin, Rangel *et al.* (1994) defined three mega-sequences within what would be eventually called the Lagoa Feia Group: K30, K40 and K50. These K-sequences were further refined by Winter *et al.* (2007) with the following subdivision being proposed: K36 (Itabapoana-Atafona Fms.), K38 (Coquinas Fm.), K46, K48 (Itabapoana-Gargaú-Macabu Fms.) and K50

(Retiro Salt Fm.). The absence of age-diagnostic fossils in the continental strata prevented these sequences being calibrated to the International Geologic Time Scale available at the time and were instead tied to local Brazilian chronostratigraphic stages (Winter *et al.* 2007). Although there is no formally published definition of these K-sequences, they are remarkably similar to the published K-sequence scheme of North-West Europe (Copestake *et al.* 2003), which is robustly calibrated to the Geologic Time Scale through marine macro- and microfossil biostratigraphies. For the Gabon wells, the sequence stratigraphic scheme of Bate (1999) and the K-sequence scheme of Copestake *et al.* (2003) and Winter *et al.* (2007) are applied and discussed below.

The Kissenda Fm. in Well A is generally a fining-upwards sequence and is interpreted in this study as a transgressive sequence tract (TST). This sequence is equivalent to Phase 2 of the first cycle of Bate (1999) and the K10 sequence of Copestake *et al.* (2003), being assigned to the Valanginian, and corresponding with the Weissert $\delta^{13}C$ event and Ostracod Zones AS2/3 – AS4. The overlying Lucina Fm. is assigned in this study to a highstand systems tract (HST) and corresponds to Phase 3 of Bate (1999) and the K20 sequence of Copestake *et al.* (2003) and is Early Hauterivian in age. A hiatus is interpreted at the top of the Lucina Fm.; this hiatus corresponds with the sequence boundary marking the top of the HST (**Figure 2**) and accounts for the absence of Ostracod Zone AS6 in Well A. Sequences K32 and K34 are inferred to be missing at the hiatus in Well A and may be part of the LST that is characterized elsewhere by the occurrence of Lucina turbidite sandstones (e.g., Smith, 1994).

The Melania Fm. is generally fining-upwards from the Melania sandstone member to the Melania Shale Mb., with the maximum lake level picked at the limestone bed at a 422m depth. The maximum lake level appears to correspond with the common abundance of the algal cysts and the freshwater dinoflagellate cyst *Loboniella hirsuta* (see supplemental datafile). The transgressive Melania Fm. interval corresponds with Phase 5 (cycle 2) of Bate (1999) and is equivalent to the Barremian K36 and K38 sequences (Copestake *et al.* 2003; Winter *et al.* 2007).

Following maximum lake levels, the fluvial-deltaic Dentale Fm. system progrades during a HST and corresponds with Phase 6 (middle of cycle 2) of Bate (1999); this is bounded at its top by a regional sequence boundary. This sequence boundary is usually associated with the base of the Gamba Sandstone Mb (base Gamba unconformity), however there is some uncertainty in its placement, particularly offshore, where the base of the Gamba may become conformable with the underlying Dentale Fm. The Dentale Fm. is Late Barremian to Early Aptian in age based on the $\delta^{13}C$ stratigraphy and assignment to Ostracod zones AS9 – AS10 and corresponds with the K38 sequence of Copestake *et al.* (2003) and Winter *et al.* (2007). Above this sequence boundary, the LST is characterized by channelized fluvial Gamba sandstones corresponding with Phase 7 (upper cycle 2) of Bate (1999) and is Early Aptian in age based on identification of the $\delta^{13}C$ Segment C7 and corresponding Palynological Zone C IX. This interval is assigned to sequences K40 (Gamba Sandstone Mb.) and K45 (Vembo Shale Mb.) after Copestake *et al.* (2003), or equivalent to sequences K46-K48 of Winter *et al.* (2007). The overlying Ezanga Fm. salt is assigned in this study to the late LST and corresponds with the K50 sequence. It is interesting to note that the K50 sequence is calibrated in the North Sea Basin to both the *Parahoplites nutfieldiensis* Boreal ammonite zone (Copestake *et al.* 2003) and the $\delta^{13}C$ C8 segment (Eldrett and Vieira, 2022), corresponding to an age of ~118 Ma (Gradstein *et al.* 2020). Given the inherent uncertainty in calibrating and correlating sequences from NW Europe to those in the South Atlantic, it remains surprising that the base of the Ezanga Fm., and the associated K50 sequence are assigned a not too dissimilar age of 118.4 Ma (earliest Late Aptian) based on the correlation of the Ezanga Fm. $\delta^{13}C$ profile to $\delta^{13}C$ segment C8 (Menegatti *et al.* 1998; Herrle *et al.* 2015: calibrated to Gradstein *et al.* 2020). This age assignment for the deposition of the salt in offshore Gabon has significant implications for regional climate and stratigraphic evolution of the South Atlantic and hydrocarbon play potential of the Pre-Salt rift sequences. It is therefore critical to provide a regional assessment of the timing of salt deposition.

5.4. Regional assessment on the timing of salt deposition in the South Atlantic

Considerable debate exists regarding the age of the salt deposition in the Early Cretaceous rift sequences of the South Atlantic, with proposed ages falling within two camps: A Late Aptian-Albian age (115 - 100 Ma) and an Early Aptian age (>117 - 123 Ma), with a total uncertainty range of ~23 Myr. These age differences partly reflect the marked disagreement between radiometric ages (i.e., Dias *et al.* 1994*;* Gomes *et al.* 2015; Szatmari and Milani, 2016; Szatmari et al. 2021) that are consistently younger than the biostratigraphically and geochemically based ages (i.e., Davison, 2007; Bengtson, 2007; Tedeschi *et al.* 2017; 2019; Bengtson *et al.* 2018) when compared to recent Geological Time Scales: Gradstein *et al.* 2012; Ogg *et al.* 2016; Gradstein *et al.* 2020).

The results and interpretations based on carbon isotope stratigraphy and biostratigraphic data from offshore Gabon indicate salt deposition initiated in the studied wells ~118.4 Ma, which is near the early-late Aptian boundary (**Figure 6**). The occurrence of evaporite deposition within the $\delta^{13}C$ Segment C8 is consistent with recent studies from NE Brazilian basins: Sergipe-Alagoas (Tedeschi *et al.* 2019) and Parnaiba – São Luís (Bastos *et al.* 2020). An even older age for evaporite deposition is also proposed for Araripe Basin, with Re-Os dating of black shales interbedded within evaporites from the Ipubi Fm. indicating a Late Barremian to Early Aptian age (123 ± 3.5 Ma; Lúcio *et al.* 2020). This radiometric age has recently been challenged (Coimbra and Freire, 2021) and although the palynological (e.g., *Afropollis jardinus, Classopollis classoides, S. variverrucata;* see Coimbra *et al.* 2002; Arai and Assine, 2020) and ostracodal (e.g., *Damonella ultima, Damonella tinkoussouensis;* see Tomé *et al.* 2014) assemblages in the Santana Group are not found worldwide (see discussion in Coimbra and Freire, 2021), the assemblages are similar to those found from the Late Barremian Dentale Fm., and Early Aptian Gamba Fm. from offshore Gabon (this study; **Figures 4 and 5**). Therefore, to resolve the age of salt deposition and the timing of rifting in the Araripe Basin, an integrated stratigraphic approach is required incorporating the existing biostratigraphy (Coimbra *et al.* 2002; Neumann *et al.* 2003; Heimhofer & Hochuli, 2010; Tomé *et al.* 2014; Nascimento *et al.* 2017, Arai and Assine, 2020; Araripe *et al.* 2021) with the recent radiometric ages (Lúcio *et al.* 2020) and new $\delta^{13}C$ stratigraphies (i.e., Varejão *et al.* 2021). At least in the other northern basins of the incipient South Atlantic basin, it appears that the timing of salt deposition was roughly similar (near the Early-Late Aptian boundary; ~118.4 Ma). The

Further to the south in the Santos and Campos basins, the evidence in support for the age of salt deposition is highly questionable, mostly reflecting i) emphasis on a single stratigraphic discipline; ii) poor reporting and/or iii) absence of publicly available data. This is particularly an issue in several articles that reported $^{40}Ar/^{39}Ar$ geochronologic dating of Pre-Salt basalt flows that provide relatively younger ages (100 – 116 Ma) compared to the biostratigraphic constraints. In many cases, $^{40}Ar/^{39}Ar$ analyzes were conducted prior to the community driven standardization EARTHTIME initiative (Bowring *et al.* 2005), where documentation of the raw data, including monitor standard and decay constants, are required for calibration. The key studies presenting $^{40}Ar/^{39}Ar$ ages to constrain the timing of salt deposition have significant failings. These include:

- Dias *et al.* (1994) presented an $^{40}Ar/^{39}Ar$ age of 113.2 ± 0.1 Ma for a basalt sample in the Pre-Salt section from Well 1-SCS-1 (South of Santos Basin). This age was subsequently incorrectly cited by both Davison (2007) and Mohriak *et al.* (2008) to constrain the age of salt deposition. For example, Davison (2007) quoted “anhydrite and carbonates of the Ariri Formation lie unconformably above the Curumim Volcanic series in Well 1-SCS-3, which has been dated at 113.2 ± 0.1 Ma (Dias et al. 1994).” It should be noted that the $^{40}Ar/^{39}Ar$ age was from Well 1-SCS-1 and not Well 1-SCS-3 as stated by Davison (2007), and, more importantly, that Well 1-SCS-1 penetrated typical Albian post-salt calcarenites directly on top of the dated basalt but did not encounter any evaporites. Therefore, this age does not provide a constraint for the age of salt deposition. Furthermore, Dias *et al.* (1994) did not publish any data in support of this age referring to "A.M.P.Mizusaki, 1993, written information". Without the step-heating spectra, monitor standard data or decay constants this age cannot be rigorously assessed.

- Gomes *et al.* (2015) and Szatmari and Milani (2016) both report an $^{40}Ar/^{39}Ar$ age of 115.7 ± 1 Ma for a ~300m thick Pre-Salt basalt flow in the Santos Basin ("Parati Flood Basalt"); and Gomes *et al.* (2015) report an $^{40}Ar/^{39}Ar$ age of 113 Ma for a Pre-Salt volcano. These are subsequently cited in Szatmari *et al.* 2021. To our knowledge, no analytical data are publicly available for scientific scrutiny: Gomes *et al.* (2015) is an unpublished Petrobras internal report whereas Szatmari and Milani (2016) state salt deposition started by 113 Ma but did not present any supporting data.
- Szatmari *et al.* (2021) present $^{40}Ar/^{39}Ar$ heating spectra from a Sergipe potash mine analyzed with a plateau age of 110.64 ± 0.34 Ma and is used this to justify "placing the salt slightly above the Aptian/Albian boundary (113.1 Ma)" (Szatmari *et al.* 2021). This analysis was conducted at the University of Toronto in 2007 prior to the EARTHTIME initiative and has not been corrected by Szatmari *et al.* (2021) to the proposed standards. In addition, the monitor standard and decay constants used were not published by Szatmari *et al.* (2021) to enable calibration to standards. Furthermore, the step-heating spectra diagram illustrated by Szatmari *et al.* (2021) indicates that approximately 80% of the argon released is within a single heating step, which does not meet the criteria of a defined step-heating plateau (Baksi, 2018; Schaen *et al.* 2021) and should therefore be rejected.

In general, the published $^{40}Ar/^{39}Ar$ ages are systematically younger than the biostratigraphically derived ages. It is difficult to ascertain the reason for this discrepancy, as the geochronologic data has not been published for evaluation. It is widely documented that the Ar-Ar system is particularly susceptible to partial loss of radiogenic ^{40}Ar during hydrothermal alteration associated with the emplacement of the volcanic/igneous rocks and/or subsequent exposure to the migration of high-temperature pore fluids (in excess of the closure temperature) during burial, which can lead to an underestimation of the time of crystallization (Baksi, 2018; Schaen *et al.* 2021). Elevated paleo-temperatures in the Pre-Salt are indicated by exotic mineral assemblages and petrographic analyses (i.e., Lima *et al.* 2019), likely also highlighting an active Pre-Salt hydrothermal system. However, the geographic extent of high temperatures in the subsurface and the nature of the host rocks (extent of alteration) are not publicly available for the samples analyzed for $^{40}Ar/^{39}Ar$ dating by Dias *et al.* (1994), Gomes *et al.* (2015), Szatmari and Milani (2016) and Szatmari *et al.* (2021). Until complete datasets become available, the $^{40}Ar/^{39}Ar$ ages should be treated with caution. One solution to this issue is to pursue high precision U/Pb geochronology studies on zircon or baddeleyite from the basalts (e.g., Rocha *et al.* 2020; 2021).

Stratigraphic uncertainty related to the timing of salt deposition is not limited to $^{40}Ar/^{39}Ar$ geochronological methods and data. Tedeschi *et al.* (2017) analyzed the carbon isotope data, correlating evaporite deposition in the Campos and Santos basins to the Early Aptian OAE-1a interval (~120 Ma). This interpretation is much older than the available geochronological ages (as discussed above) and potentially implies that salt deposition is time equivalent to sequence K40 (Copestake *et al.* 2003; K46 after Winter *et al.* 2007), rather than K50 (as originally assigned by Winter *et al.* 2007), and coeval with the base-Gamba unconformity and associated relative lake level fall on the African margin. In addition, an older age estimate for evaporite deposition the Santos/Campos basins compared to the northern basins (i.e., Gabon, Sergipe-Alagoas, Parnaibe, São Luis) would suggest strong diachroneity in salt deposition (Tedeschi *et al.* 2017, 2019). However, these results should also be treated with caution. The $\delta^{13}C$ data presented by Tedeschi *et al.* (2017) were a composite of two wells from two different basins: CP-5 from the

Campos Basin and Well X from the Santos Basin, with the assumption of coeval salt deposition in these two basins and without biostratigraphic constraints in the Pre-Salt section to support construction of the composite reference section. In addition, the illustration and interpretation of $\delta^{13}C$ data from Well CP-5 by Tedeschi *et al.* (2017) are not entirely accurate. These data were originally analyzed and presented by Dias (1998), with the low $\delta^{13}C$ value interval that Tedeschi *et al.* (2017) tentatively correlate with $\delta^{13}C$ Segment C3 and the onset of salt deposition is actually 70m below the base of evaporites (see Dias, 1998, figures 5.12 and 5.16). Therefore, the $\delta^{13}C$ correlation cannot be used as evidence for evaporite deposition at the base of OAE-1a. Based on the $\delta^{13}C$ segment assignments of Tedeschi *et al.* (2017) to the Pre-Salt section of Well CP-5, a linear interpolation can be applied from $\delta^{13}C$ segments C1-C3 up to the base of the salt (including the un-sampled 70m interval). Under this assumption, a younger age of salt deposition can be calculated (~119.2 Ma, with a rock accumulation rate ~12.5 cm/kyr). With lower rock accumulation rates this un-sampled 70m interval from Well CP5, and therefore the age of base of the salt unit, could potentially be much younger. To resolve this uncertainty the 70m interval in Well CP-5, from the top analyzed sample at 4629m to the base evaporites at 4559m (Dias, 1998; Figure 5.17) should, if possible, be analyzed for $\delta^{13}C$ stratigraphy.

Furthermore, in supra-evaporitic sequences from the nearby well CB-3, the occurrence of the planktonic foraminifers *Hedbergella aptiana* and *H. gotbachikae* identified by Tedeschi *et al.* (2017; see supplemental figure DR-1) were used to support of an early Aptian age for evaporite deposition. However, the illustrated specimens exhibit very poor preservation and their assignment to *H. aptiana* and *H. gotbachikae* is questionable (Brian Huber pers. comms. 2022). In addition, the carbonate $\delta^{13}C$ profile from Well X in the Santos Basin is used to constrain the age of cessation of evaporite deposition, with the highest values (~3-5‰; 2756m to 2906m) correlated to post OAE-1a $\delta^{13}C$ segments C5-C7 (Early Aptian; Tedeschi *et al.* 2017). However, this interval could easily be correlated to $\delta^{13}C$ segments C10-C14 and correspond with the Aptian-Albian boundary instead; it may be noted that this possibility was also raised by Pietzsch *et al.* (2020). This uncertainty reflects the fact that this well is located in the Santos basin, ~600 km away from Well CP-5 in the Campos Basin, and without additional stratigraphic constraints uncertainties remain in the quality of this composite record and associated age assignments should be treated with caution.

In other studies, the age of salt deposition is also constrained by the age of the overlying strata. Davison (2007) interpreted an Early Aptian age for salt deposition in offshore Angola based on the occurrence above the salt of the planktonic foraminifer marker *Leupoldina cabri*. However, this evidence was from a "confidential well in one of the shelfal blocks" (Davison, 2007); because the data were not published the evidence is difficult to verify. Furthermore, Davison (2007) referred to Aptian planktonic foraminifera from DSDP Site 364, at which drilling was suspended above the salt. Subsequent re-interpretation of the biostratigraphy from DSDP Site 364 by Bruno *et al.* (2020) clearly indicates Albian nannofossil markers present. Biostratigraphy and $\delta^{13}C$ profiles from post-salt strata from the Campos Basin and offshore Gabon also indicate post-salt deposition near the Albian-Aptian boundary (*ca*. 113 Ma; Caetano-Filho *et al.* 2017; Campbell *et al.* 2019). However, the oldest strata above the salt in offshore Brazil are reported as Late Aptian from the Santos, Campos and Espírito Santo basins based on planktonic foraminifers (Sanjinés *et al.* 2022), and Early Aptian from the Sergipe Basin, based on the occurrence of the ammonite *Dufrenoyia justinae*, which is correlated with the *Epicheloniceras martini* "standard zone" (Bengtson, 2007, Bengtson *et al.* 2018). From these studies, there is large diachroneity of deposition immediately above the salt, with differential onlap and erosion (i.e., Campbell *et al.* 2019), complex geometries and the development of mini-basins during halokinesis (i.e., Guerra and Underhill, 2012). Moreover, these ages only provide constraints for deposition of sediments on top of the salt units, and therefore do not directly date the cessation of salt deposition or, critically, its inception. Additional studies are therefore required from the southern basins of the South Atlantic (i.e., Campos, Santos, Kwanza; Namibe) to constrain the timing of rifting and salt deposition before conclusions can be made regarding latitudinal diachroneity (i.e., Tedeschi *et al.* 2019).

6. Conclusions

Records of stable $\delta^{13}C$ values from bulk organic matter and insoluble kerogens were generated for the Early Cretaceous salt and Pre-Salt intervals from two wells in offshore Gabon. The recovered composite $\delta^{13}C$ profile from the two wells was integrated with palynological and ostracod biostratigraphy and placed within a sequence stratigraphic framework, providing constraints onto the timing of lake/margin evolution and salt deposition. The correlation between the offshore Gabon $\delta^{13}C$ profile and other published sections that are calibrated to GTS2020, as well as other regional sections from NE Brazil, supports the reliability of the $\delta^{13}C$ record generated from the Gabon wells. A positive $\delta^{13}C$ shift identified in the Kissenda Fm. is proposed here to correspond with the Valanginian Weissert $\delta^{13}C$ event. The Melania to Dentale intervals correspond with the Barremian transgressive and highstand systems tracts, with the Barremian-Aptian boundary assigned to strata from the uppermost Dentale Fm (near the base of $\delta^{13}C$ Segment C2). The Early Aptian OAE-1a event ($\delta^{13}C$ Segments C3 – C6) is missing in the unconformity at the base of the Gamba Sandstone Mb.

The Gamba Fm. exhibits positive $\delta^{13}C$ values assigned to $\delta^{13}C$ Segment C7, with salt deposition of the Ezanga Fm. occurring within $\delta^{13}C$ Segment C8 (~118.4 Ma to 116.8; Early-Late Aptian; Gradstein *et al.* 2020). This age for the initiation of salt deposition in offshore Gabon is consistent with other northern rift salt basins (Sergipe-Alagoas, Parnaiba, São Luis) and provides additional constraint for timing of the opening of the South Atlantic. It should be noted, however, that the data and interpretations provided here are just a snapshot from only two wells and that lateral variation in the timing of rifting and salt deposition within basins, particularly between proximal and distal domains, is expected. These age estimates are therefore likely be further refined with additional studies.

The age of salt deposition in the southern basins (Campos, Santos) is also evaluated to determine potential latitudinal diachroneity. However, the interpretations for the age of the salt in these basins are much more controversial, with significant problems and uncertainties in some key lines of evidence. We conclude that the published $^{40}Ar/^{39}Ar$ ages are difficult to evaluate, as the raw data are not publicly available, and the few available step-heating spectra do not appear to reach a statistically reliable plateau. It is likely that $^{40}Ar/^{39}Ar$ dating is limited by the relatively low closure temperature of the Ar-system, being potentially affected by hydrothermal alteration, resulting in systematically younger ages than those provided by biostratigraphy and $\delta^{13}C$ stratigraphy in these basins. However, the published ages inferred from biostratigraphic data and $\delta^{13}C$ stratigraphy are also challenged. In all cases, publicly available stratigraphic data is also geographically limited, preventing a full spatial-temporal understanding of rift evolution of the South Atlantic. Therefore, the data from offshore Gabon provide important age constraints and stratigraphic contributions to the ongoing debate of the timing of salt deposition in the South Atlantic.

Acknowledgements

We like to thank Rob Campbell and Nina Liefhebber-Bonis for taxonomic discussions and logistical support. Lorcan Kennan, Ken McDermott and Susanne Witte are thanked for discussions on regional geology. We acknowledge the feedback from internal review by Mark

Hollanders, Brent Wignall, Colin Grant and Olaf Podlaha as well as external peer review by James Doyle and an anonymous reviewer, which improved the manuscript. Permission to publish the data and interpretations herein were kindly provided by Shell International Exploration and Production B.V. The interpretations and opinions presented here are those of the authors only and do not in any way represent the views of Shell International Exploration and Production B.V./Shell Global Solutions International B.V..

References:

Alley, N.F., Hore, S.B. and Frakes, L.A., 2020. Glaciations at high-latitude Southern Australia during the Early Cretaceous. *Australian Journal of Earth Sciences*, *67*(8), pp.1045-1095.

Ando, A., Kakegawa, T., Takashima, R. and Saito, T., 2002. New perspective on Aptian carbon isotope stratigraphy: data from δ13C records of terrestrial organic matter. Geology, 30(3), pp.227-230.

Bastos, L. P. H., Pereira, E., da Costa Cavalcante, D., Alferes, C. L. F., de Menezes, C. J., & Rodrigues, R. 2020. Expression of Early Cretaceous global anoxic events in Northeastern Brazilian basins. *Cretaceous Research*, *110*, 104390.

Arai, M. and Assine, M.L., 2020. Chronostratigraphic constraints and paleoenvironmental interpretation of the Romualdo Formation (Santana Group, Araripe Basin, Northeastern Brazil) based on palynology. *Cretaceous Research,* 116, pp.104-610

Araripe, R. C., Oliveira, D. H., Tome, M. E., de Mello, R. M., & Barreto, A. M. (2021). Foraminifera and Ostracoda from the lower Cretaceous (Aptian–lower Albian) Romualdo formation, Araripe basin, northeast Brazil: Paleoenvironmental inferences. Cretaceous Research, 122, 104766.

Bate, R.H., 1999. Non-marine ostracod assemblages of the Pre-Salt rift basins of West Africa and their role in sequence stratigraphy. *Geological Society, London, Special Publications*, 153(1), pp.283-292.

Bengtson, P., Zucon, M.H. and Sobral, A.D.C.S., 2018. Cretaceous ammonite zonation of the Sergipe Basin, northeastern Brazil. *Cretaceous Research*, 88, pp.111-122.

Bengtson, P., Koutsoukos, E.A., Kakabadze, M.V. and Zucon, M.H., 2007. Ammonite and foraminiferal biogeography and the opening of the Equatorial Atlantic Gateway. In *1er Symposium International de Paleeobiogéographie, Résumés* (Vol. 12).

Bergman, S.C., Eldrett, J.S. and Minisini, D. 2021. Phanerozoic Large Igneous Province, petroleum system, and source rock links. In *Large Igneous Provinces* (eds R.E. Ernst, A.J. Dickson and A. Bekker). https://doi.org/10.1002/9781119507444.ch9

Black, B. A. and Gibson, S. A., 2019. Deep carbon and the life cycle of large igneous provinces. *Elements,* 15, 319–324.

Bodin, S., Meissner, P., Janssen, N. M., Steuber, T. and Mutterlose, J. 2015. Large igneous provinces and organic carbon burial: Controls on global temperature and continental weathering during the Early Cretaceous. *Global and Planetary Change,* 133, pp. 238-253.

Bowring, S.A., Erwin, D., Parrish, R. and Renne, P., 2005. EARTHTIME: A community-based effort towards high-precision calibration of earth history. *Geochimica et Cosmochimica Acta,* 69, pp. A316-A316.

Bralower, T.J., CoBabe, E., Clement, B., Sliter, W.V., Osburn, C.L. and Longoria, J., 1999. The record of global change in mid-Cretaceous (Barremian-Albian) sections from the Sierra Madre, northeastern Mexico. *The Journal of Foraminiferal Research*, *29*(4), pp.418-437.

Bralower, T.J., Sliter, W.V., Arthur, M.A., Leckie, R.M., Allard, D. and Schlanger, S.O., 1993. Dysoxic/anoxic episodes in the Aptian-Albian (Early Cretaceous). *The Mesozoic Pacific: Geology, Tectonics, and Volcanism:* Washington, DC, *American Geophysical Union, Geophysical Monograph*, *77*, pp.5-37.

Brune, S., Williams, S.E. and Müller, D.R., 2017. Potential links between continental rifting, CO_2 degassing and climate change through time." *Nature Geoscience,* 2017. https://doi.org/10.1038/s41561-017-0003-6.

Bruno, M.D.R., Fauth, G., Watkins, D.K. and Savian, J.F., 2020. Albian–Cenomanian calcareous nannofossils from DSDP Site 364 (Kwanza Basin, Angola): Biostratigraphic and paleoceanographic implications for the South Atlantic. *Cretaceous Research*, *109*, pp.104377.

Caetano-Filho, S., Dias-Brito, D., Rodrigues, R. and de Azevedo, R. L. M. 2017. Carbonate microfacies and chemostratigraphy of a late Aptian–early Albian marine distal section from the primitive South Atlantic (SE Brazilian continental margin): Record of global ocean-climate changes?. *Cretaceous Research*, *74*, pp. 23-44.

Campbell, R., Liefhebber-Bonis, N.R., Eldrett, J.S., Jakeman, M.D. 2019. Post-Salt stratigraphy of the Léopard Prospect, Deepwater Gabon. *SEPM Special Publications* 111.

Ceraldi, T.S. and Green, D., 2017. Evolution of the South Atlantic lacustrine deposits in response to Early Cretaceous rifting, subsidence and lake hydrology. *Geological Society, London, Special Publications*, 438(1), pp.77-98.

Coccioni, R. and Galeotti, S., 2003. The mid-Cenomanian Event: prelude to OAE 2. *Palaeogeography, Palaeoclimatology, Palaeoecology*, *190*, pp.427-440.

Coimbra, J.C., Arai, M. and Carreño, A.L., 2002. Biostratigraphy of Lower Cretaceous microfossils from the Araripe basin, northeastern Brazil. *Geobios, 35*(6), pp.687-698.

Coimbra, J. C., & Freire, T. M. (2021). Age of the Post-rift Sequence I from the Araripe Basin, Lower Cretaceous, NE Brazil: implications for spatio-temporal correlation. *Revista Brasileira de Paleontologia*, *24*(1), pp. 37-46.

Copestake, P., Sims, A.P., Crittenden, S., Hamar, G.P., Ineson, J.R., Rose, P.T. and Tringham, M.E., 2003. Lower Cretaceous. *The Millennium Atlas: Petroleum Geology of the Central and Northern North Sea. Geological Society, London*, *191*, pp.211.

Davison, I., 2007. Geology and tectonics of the South Atlantic Brazilian salt basins. *Geological Society, London, Special Publications*, *272*(1), pp.345-359.

D'Hondt, S., Rutherford, S., Spivack, A.J., 2002. Metabolic activity of subsurface life in deep-sea sediments. *Science* 295, 2067–2070

Dias, J.L., 1998. Análise sedimentológica e estratigráfica do andar aptiano em parte da margem leste do Brasil e no Platô das Malvinas: considerações sobre as primeiras incursões e ingressões marinhas do Oceano Atlântico Sul Meridional. *Brazil.* Unpublished PhD thesis. *Universidade Federal do Rio Grande do Sul*.

Dias, J.L., Sad, A.R.E., Fontana, R.L. and Feijó, F.J. 1994. Bacia de Pelotas: *Boletim de Geociências da Petrobras*, v. 8, pp. 235–245.

Dickson, A.J., Cohen, A.S., Davies, M., 2021. The osmium isotope signature of Phanerozoic Large Igneous Provinces. In Large Igneous Provinces (eds R.E. Ernst, A.J. Dickson and A. Bekker). https://doi.org/10.1002/9781119507444.ch10.

Doyle, J.A., Biens, P, Doerenkamp, A. and Jardiné, S. 1977. Angiosperm pollen from the pre-Albian Lower Cretaceous of equatorial Africa. *Bulletin des Centres de Recherches Exploration-Production Elf-Aquitaine,* pp. 451-473

Doyle, J.A., Jardiné, S and Doerenkamp, A. 1982. *Afropollis*, a new genus of early angiosperm pollen, with notes on the Cretaceous palynostratigraphy and paleoenvironments of northern Gondwana. *1982 Soc. Nat. Elf Aquitaine (Production),* pp. 40-1117.

Doyle, J.A., 1992. Revised palynological correlations of the lower Potomac Group (USA) and the Cocobeach sequence of Gabon (Barremian-Aptian). *Cretaceous Research*, *13*(4), pp.337-349.

Eldrett, J.S. and Vieira, M. (in review). An integrated carbon isotope and bio-sequence stratigraphic study of the Early Cretaceous to Paleogene, Central North Sea. *Marine and Petroleum Geology,* 141, 105696.

Fairhead, J.D., 1988. Mesozoic plate tectonic reconstructions of the central South Atlantic Ocean: the role of the West and Central African rift system. *Tectonophysics*, 155(1-4), pp.181-191.

Farias, F., Szatmari, P., Bahniuk, A. and Franca, A.B., 2019. Evaporitic carbonates in the Pre-Salt of Santos Basin–Genesis and tectonic implications. *Marine and Petroleum Geology*, *105*, pp.251-272.

Foster, G. L., Royer, D. L., & Lunt, D. J., 2017. Future climate forcing potentially without precedent in the last 420 million years. *Nature Communications,* 8(1), pp.1-8.

Friedrich, O., Norris, R.D. and Erbacher, J., 2012. Evolution of middle to Late Cretaceous oceans—a 55 my record of Earth's temperature and carbon cycle. *Geology*, *40*(2), pp.107-110.

Gomes, L.C., Lima, F.M., Vieira, I.S., Lobo, J.T *et al.* 2015. Magmatismo Jiquiá e Alagoas na Bacia de Santos. *Petrobras. Relatório Interno*, Rio de Janeiro (2015)

Gradstein, F. M., Ogg, J. G., Schmitz, M. D. and Ogg, G. M. (Eds.). 2020. *Geologic Time Scale 2020*. Elsevier.

Gradstein, F.M., Ogg, J.G., Schmitz, M.D. and Ogg, G.M. (Eds.). 2012. *The Geologic Time Scale 2012*. Elsevier.

Gröcke, D.R., Price, G.D., Robinson, S.A., Baraboshkin, E.Y., Mutterlose, J. and Ruffell, A.H., 2005. The Upper Valanginian (Early Cretaceous) positive carbon–isotope event recorded in terrestrial plants. *Earth and Planetary Science Letters*, *240*(2), pp.495-509.

Grosdidier, E., Braccini, E., Dupont, G. and Moron, J.M., 1996. Biozonation du Crétacé Inférieur non marin des bassins du Gabon et du Congo. *Bulletin des Centres de Recherches Exploration-Production Elf-Aquitaine. Mémoire*, (16), pp.67-82.

Guerra, M. C. and Underhill, J. R., 2012. Role of halokinesis in controlling structural styles and sediment dispersal in the Santos Basin, offshore Brazil. *Geological Society, London, Special Publications*, *363*(1), pp.175-206.

Hay, W.W., 2017. Toward understanding Cretaceous climate—An updated review. *Science China Earth Sciences*, *60*(1), pp.5-19.

Heimhofer, U., P. A. Hochuli, 2010. Early Cretaceous angiosperm pollen from a low-latitude succession (Araripe Basin, NE Brazil). *Rev. Palaeobot. Palynol.* 161: 105-126.

Heine, C., Zoethout, J. and Müller, R.D., 2013. Kinematics of the South Atlantic rift. *Solid Earth*, *4*(2), pp.215-253.

Herrle, J.O., Kößler, P., Friedrich, O., Erlenkeuser, H. and Hemleben, C., 2004. High-resolution carbon isotope records of the Aptian to Lower Albian from SE France and the Mazagan Plateau (DSDP Site

545): a stratigraphic tool for paleoceanographic and paleobiologic reconstruction. *Earth and Planetary Science Letters*, *218*(1-2), pp.149-161.

Herrle, J.O., Schröder-Adams, C.J., Davis, W., Pugh, A.T., Galloway, J.M. and Fath, J., 2015. Mid-Cretaceous High Arctic stratigraphy, climate, and oceanic anoxic events. *Geology*, *43*(5), pp.403-406.

Huber, B.T., Norris, R.D. and MacLeod, K.G., 2002. Deep-sea paleotemperature record of extreme warmth during the Cretaceous. *Geology*, *30*(2), pp.123-126.

Jenkyns, H.C., 2010. Geochemistry of oceanic anoxic events. *Geochemistry, Geophysics, Geosystems*, *11*(3).

Johansson, L., Zahirovic, S and Müller, D, R., 2018. The Interplay between the eruption and weathering of Large Igneous Provinces and the deep- time carbon cycle. *Geophysical Research Letters*, 45(11), pp. 5380–5389.

Kessels, K., Mutterlose, J. and Michalzik, D., 2006. Early Cretaceous (Valanginian-Hauterivian) calcareous nannofossils and isotopes of the northern hemisphere: proxies for the understanding of Cretaceous climate. *Lethaia*, *39*(2), pp.157-172.

Koutsoukos, E.A., Destro, N., de Azambuja Filho, N.C. and Spadini, A.R., 1993. Chapter 11: Upper Aptian-Lower Coniacian Carbonate Sequences in the Sergipe Basin, Northeastern Brazil. *In:* Simo, T., Scott, R.W and Masse, J-P. (Eds) Cretaceous carbonate platforms. *AAPG Memoir* 56, pp. 127-144.

Hyunwoo, L., Muirhead, J.D., Fischer, T.B., Ebinger, C.J., Kattenhorn, S.A., Sharp, Z.D and Kianji, G., 2016. Massive and prolonged deep carbon emissions associated with continental rifting. *Nature Geoscience* 9, no. 2: pp.145–149. https://doi.org/10.1038/ngeo2622.

Lima, B. E. M. and De Ros, L. F., 2019. Deposition, diagenetic and hydrothermal processes in the Aptian Pre-Salt lacustrine carbonate reservoirs of the northern Campos Basin, offshore Brazil. *Sedimentary Geology*, *383*, pp. 55-81.

Littler, K., Robinson, S.A., Bown, P.R., Nederbragt, A.J. and Pancost, R.D., 2011. High sea-surface temperatures during the Early Cretaceous Epoch. *Nature Geoscience*, *4*(3), pp.169-172.

Lúcio, T., Neto, J. A. S. and Selby, D., 2020. Late Barremian/Early Aptian Re–Os age of the Ipubi Formation black shales: Stratigraphic and paleoenvironmental implications for Araripe Basin, northeastern Brazil. *Journal of South American Earth Sciences*, *102*, 102699.

Luo, G., Kump, L. R., Wang, Y., Tong, J., Arthur, M. A., Yang, H., ... & Xie, S. (2010). Isotopic evidence for an anomalously low oceanic sulfate concentration following end-Permian mass extinction. *Earth and Planetary Science Letters*, *300*(1-2), pp.101-111.

Mather, T. A. and Schmidt, A., 2021. Environmental effects of volcanic volatile fluxes from subaerial Large Igneous Provinces, In Large Igneous Provinces (eds R.E. Ernst, A.J. Dickson and A. Bekker). https://doi.org/10.1002/9781119507444.ch4.

Mbina Mounguengui, M. and Guiraud, M., 2009. Neocomian to early Aptian syn-rift evolution of the normal to oblique-rifted north Gabon margin (interior and N'Komi basins). *Marine and Petroleum Geology* 26, no. 6, pp.1000–1017. https://doi.org/10.1016/j.marpetgeo.2008.11.001.

Menegatti, A.P., Weissert, H., Brown, R.S., Tyson, R.V., Farrimond, P., Strasser, A. and Caron, M., 1998. High-resolution δ13C stratigraphy through the Early Aptian "Livello selli" of the Alpine tethys. *Paleoceanography*, *13*(5), pp.530-545.

Mills, J. V., Gomes, M. L., Kristall, B., Sageman, B. B., Jacobson, A. D., & Hurtgen, M. T. (2017). Massive volcanism, evaporite deposition, and the chemical evolution of the Early Cretaceous ocean. *Geology*, *45*(5), pp.475-478.

Mohriak, W., Nemčok, M. and Enciso, G., 2008. South Atlantic divergent margin evolution: rift-border uplift and salt tectonics in the basins of SE Brazil. *Geological Society, London, Special Publications*, *294*(1), pp.365-398.

Moulin, M., Aslanian, D. and Unternehr, P., 2010. A new starting point for the south and equatorial Atlantic Ocean. *Earth Science Reviews* 98, 1–2: pp.1–37. https://doi.org/10.1016/j.earscirev.2009.08.001.

Mutterlose, J., Malkoc, M., Schouten, S., Damsté, J.S.S. and Forster, A., 2010. TEX86 and stable $\delta^{18}O$ paleothermometry of early Cretaceous sediments: Implications for belemnite ecology and paleotemperature proxy application. *Earth and Planetary Science Letters*, *298*(3-4), pp.286-298.

Müller, D, R., Zahirovic, S., Williams, S.E., Cannon, J., Seton, M., Bower, D.J., Tetley, M., Heine, C., Le Breton, E., Liu, S., Russell, S.H.J., Yang, T., Leonard, J. and Gurnis, M., 2019. A global plate model including lithospheric deformation along major rifts and orogens since the Triassic. *Tectonics* 38 (6), pp.1884-1907. https://doi.org/10.1029/2018TC005462.

Nascimento, L.R., Tomé, M.E., Barreto, A.M., de Oliveira, D.H. and Neumann, V.H., 2017. Biostratigraphic analysis based on palynomorphs and ostracods from core 2-JNS-01PE, Lower Cretaceous, Jatobá Basin, northeastern Brazil. *Journal of South American Earth Sciences*, *76*, pp.115-136.

Neuharth, D., Brune, S., Glerum, A., Heine, C., & Welford, J. K., 2021. Formation of continental microplates through rift linkage: Numerical modeling and its application to the Flemish Cap and Sao Paulo Plateau. *Geochemistry, Geophysics, Geosystems*, 22(4), e2020GC009615.

Neumann, V.H., Borrego, A.G., Cabrera, L. and Dino, R., 2003. Organic matter composition and distribution through the Aptian–Albian lacustrine sequences of the Araripe Basin, northeastern Brazil. *International Journal of Coal Geology*, *54*(1-2), pp.21-40.

O'Brien, C.L., Robinson, S.A., Pancost, R.D., Damste, J.S.S., Schouten, S., Lunt, D.J., Alsenz, H., Bornemann, A., Bottini, C., Brassell, S.C. and Farnsworth, A., 2017. Cretaceous sea-surface temperature evolution: Constraints from TEX86 and planktonic foraminiferal oxygen isotopes. *Earth-Science Reviews*, *172*, pp.224-247.

Oehlert, A.M. and Swart, P.K., 2014. Interpreting carbonate and organic carbon isotope covariance in the sedimentary record. *Nature Communications*, *5*(1), pp.1-7.

Ogg, J.G., Ogg, G.M. and Gradstein, F.M., 2016. *A Concise Geologic Time Scale: 2016*. Elsevier.

Percival, L.M.E., Tedeschi, L.R., Creaser, R.A., Bottini, C., Erba, E., Giraud, F., Svensen, H., Savian, J., Trindade, R., Coccioni, R. and Frontalini, F., 2021. Determining the style and provenance of magmatic activity during the Early Aptian Oceanic Anoxic Event (OAE 1a). *Global and Planetary Change*, p.103461.

Pietzsch, R., Oliveira, D.M., Tedeschi, L.R., Neto, J.V.Q., Figueiredo, M.F., Vazquez, J.C. and de Souza, R.S., 2018. Palaeohydrology of the Lower Cretaceous Pre-Salt lacustrine system, from rift to post-rift phase, Santos Basin, Brazil. *Palaeogeography, Palaeoclimatology, Palaeoecology*, *507*, pp.60-80.

Pietzsch, R., Tedeschi, L.R., Oliveira, D.M., dos Anjos, C.W.D., Vazquez, J.C. and Figueiredo, M.F., 2020. Environmental conditions of deposition of the Lower Cretaceous lacustrine carbonates of the Barra Velha Formation, Santos Basin (Brazil), based on stable carbon and oxygen isotopes: a continental record of pCO2 during the onset of the Oceanic Anoxic Event 1a (OAE 1a) interval? *Chemical Geology*, *535*, 119457.

Poropat, S.F. and Colin, J.P., 2012. Early Cretaceous ostracod biostratigraphy of eastern Brazil and western Africa: An overview. *Gondwana Research*, 22(3-4), pp.772-798.

Price, G.D., Ruffell, A.H., Jones, C.E., Kalin, R.M. and Mutterlose, J., 2000. Isotopic evidence for temperature variation during the early Cretaceous (late Ryazanian–mid-Hauterivian). *Journal of the Geological Society*, *157*(2), pp.335-343.

Quan, T. M., & Adeboye, O. O., 2021. Interpretation of nitrogen isotope profiles in petroleum systems: A review. *Frontiers Earth Science* 9, 705691.

Rangel, H.D., Martins, F.A., Esteves, F.R. and Feijo, F.J., 1994. Campos Basin; Bacia de Campos. *Boletim de Geociencias da Petrobras*, *8*.

Rabinowitz, P.D. and LaBrecque, J., 1979. The Mesozoic South Atlantic Ocean and evolution of its continental margins. *Journal of Geophysical Research: Solid Earth,* 84(B11), pp.5973-6002.

Robinson, R. S., Kienast, M., Luiza Albuquerque, A., Altabet, M., Contreras, S., De Pol Holz, R., *et al.* 2012. A review of nitrogen isotopic alteration in marine sediments. *Paleoceanography*. 27, PA4203. doi:10.1029/2012pa002321

Rocha, B. C., Davies, J. H., Janasi, V. A., Schaltegger, U., Nardy, A. J., Greber, N. D., Lucchetti, A.F., Polo, L. A., 2020. Rapid eruption of silicic magmas from the Paraná magmatic province (Brazil) did not trigger the Valanginian event. *Geology*, 48(12), pp.1174-1178.

Rocha, B. C., Gaynor, S. P., de Assis Janasi, V., Davies, J. H., Florisbal, L. M., Waichel, B. L., Schaltegger, U., 2021. The mafic intrusive magmatism from the Paraná LIP constrained by new U-Pb baddeleyite ID-TIMS ages. Goldschmidt Conference Abstract, 2021, Virtual, 4-9 July. https://doi.org/10.7185/gold2021.7228

Royer, D.L., Pagani, M. and Beerling, D.J., 2012. Geobiological constraints on Earth system sensitivity to CO2 during the Cretaceous and Cenozoic. *Geobiology*, *10*(4), pp.298-310.

Saller, A., Rushton, S., Buambua, L., Inman, K., McNeil, R. and Dickson, J.T., 2016. Presalt stratigraphy and depositional systems in the Kwanza Basin, offshore Angola. *AAPG Bulletin*, *100*(7), pp.1135-1164.

Sanjinés, A. E. S., Viviers, M. C., Costa, D. S., dos Anjos Zerfass, G. D. S., Beurlen, G., & Strohschoen Jr, O. (2022). Planktonic foraminifera from the Aptian section of the Southeastern Brazilian Atlantic margin. *Cretaceous Research,* 105141.

Schlanger, S.O. and Jenkyns, H.C., 1976. Cretaceous oceanic anoxic events: causes and consequences. *Netherlands Journal of Geosciences/Geologie en Mijnbouw*, (Classic Papers), 55 (3-4), pp.179–84.

Scotese, C.R., Gahagan, L.M. and Larson, R.L., 1988. Plate tectonic reconstructions of the Cretaceous and Cenozoic ocean basins. *Tectonophysics,* 155(1-4), pp.27-48.

Scotese, C.R., Song, H., Mills, B.J.W., van der Meer, D.G., 2021. Phanerozoic paleotemperatures: The earth’s changing climate during the last 540 million years. *Earth-Science Reviews* 215, 103503, https://doi.org/10.1016/j.earscirev.2021.103503.

Smith, R.D.A., 1995. Reservoir architecture of syn-rift lacustrine turbidite systems, early Cretaceous, offshore South Gabon. *Geological Society, London, Special Publications*, *80*(1), pp.197-210.

Steinig, S., Dummann, W., Park, W., Latif, M., Kusch, S., Hofmann, P. and Flögel, S., 2020. Evidence for a regional warm bias in the Early Cretaceous TEX86 record. *Earth and Planetary Science Letters*, *539*, 116184.

Szatmari, P. and Milani, E.J., 2016. Tectonic control of the oil-rich large igneous-carbonate-salt province of the South Atlantic rift. *Marine and Petroleum Geology*, *77*, pp.567-596.

Szatmari, P., de Lima, C.M., Fontaneta, G., de Melo Lima, N., Zambonato, E., Menezes, M.R., Bahniuk, J., Coelho, S.L., Figueiredo, M., Florencio, C.P. and Gontijo, R., 2021. Petrography, geochemistry and origin of South Atlantic evaporites: The Brazilian side. *Marine and Petroleum Geology*, *127*, 104805.

Szpak, P., Metcalfe, J.Z. and Macdonald, R.A., 2017. Best practices for calibrating and reporting stable isotope measurements in archaeology. *Journal of Archaeological Science*: Reports, 13, pp.609-616.

Tedeschi, L.R., Jenkyns, H.C., Robinson, S.A., Sanjinés, A.E., Viviers, M.C., Quintaes, C.M. and Vazquez, J.C., 2017. New age constraints on Aptian evaporites and carbonates from the South Atlantic: Implications for Oceanic Anoxic Event 1a. *Geology*, *45*(6), pp.543-546.

Tedeschi, L.R., Jenkyns, H.C., Robinson, S.A., Lana, C.C., Menezes Santos, M.R.F. and Tognoli, F.M., 2019. Aptian carbon-isotope record from the Sergipe-Alagoas Basin: New insights into oceanic anoxic event 1a and the timing of seawater entry into the South Atlantic. *Newsletters on Stratigraphy*.

Tomé, M.E., Lima Filho, M.F. and Neumann, V.H., 2014. Taxonomic studies of non-marine ostracods in the Lower Cretaceous (Aptian–lower Albian) of post-rift sequence from Jatobá and Araripe basins (Northeast Brazil): stratigraphic implications. *Cretaceous Research*, *48*, pp.153-176.

Torsvik, T. H., Rousse, S., Labails, C. and Smethurst, M.A., 2009. A new scheme for the opening of the south Atlantic Ocean and the dissection of an Aptian salt basin. *Geophysical Journal International* 177, no. 3, 1315–33. https://doi.org/10.1111/j.1365-246X.2009.04137.x.

Tyson, R.V., 1995. *Sedimentary Organic Matter,* First Edition (pp. 615). Chapman and Hall, London. U.K.

van Roij, L., Sluijs, A., Laks, J. J., & Reichart, G. J., 2017. Stable carbon isotope analyses of nanogram quantities of particulate organic carbon (pollen) with laser ablation nano combustion gas chromatography/isotope ratio mass spectrometry. *Rapid Communications in Mass Spectrometry,* 31(1), 47-58.

Valentine, D.L., 2002. Biogeochemistry and microbial ecology of methane oxidation in anoxic environments: a review. *Antonie Leeuwenhoek* 81, 271–282.

Varejão, F. G., Warren, L. V., Simões, M. G., Buatois, L. A., Mángano, M. G., Bahniuk Rumbelsperger, A. M., & Assine, M. L., 2021. Mixed siliciclastic–carbonate sedimentation in an evolving epicontinental sea: Aptian record of marginal marine settings in the interior basins of north-eastern Brazil. *Sedimentology* 68 (5), pp. 2125-2164.

Vickers, M.L., Price, G.D., Jerrett, R.M. and Watkinson, M., 2016. Stratigraphic and geochemical expression of Barremian–Aptian global climate change in Arctic Svalbard. *Geosphere*, *12*(5), pp.1594-1605.

Wang, L., Song, Z., Cao, X., & Li, Y. (2015). Compound-specific carbon isotope study on the hydrocarbon biomarkers in lacustrine source rocks from Songliao Basin. Organic Geochemistry, 87, 68-77.

Wang, Y., Huang, C., Sun, B., Quan, C., Wu, J. and Lin, Z., 2014. Paleo-CO2 variation trends and the Cretaceous greenhouse climate. *Earth-Science Reviews*, *129*, pp.136-147.

Weissert, H., Lini, A., Föllmi, K.B. and Kuhn, O., 1998. Correlation of Early Cretaceous carbon isotope stratigraphy and platform drowning events: a possible link? *Palaeogeography, Palaeoclimatology, Palaeoecology*, *137*(3-4), pp.189-203.

Winter, W.R., Jahnert, R.J. and França, A.B., 2007. Bacia de Campos. *Boletim de Geociencias da Petrobras 15*(2), pp.511-529.

Wortmann, U. G., & Chernyavsky, B. M. 2007. Effect of evaporite deposition on Early Cretaceous carbon and sulphur cycling. *Nature*, *446*(7136), pp.654-656.

Wortmann, U. G., & Paytan, A. 2012. Rapid variability of seawater chemistry over the past 130 million years. *Science*, *337*(6092), pp.334-336.

Zhang, X., Zhang, G. and Sha, J., 2016. Lacustrine sedimentary record of early Aptian carbon cycle perturbation in western Liaoning, China. *Cretaceous Research*, *62*, pp.122-129.

Zhang, X., Li, S., Wang, X., Zhao, X. and Yin, T., 2021. Expression of the early Aptian Oceanic Anoxic Event (OAE) 1a in lacustrine depositional systems of East China. *Global and Planetary Change*, *196*, 103370.